Analysis of the Slab Ocean El Nino Atmospheric Feedbacks in Observed and Simulated ENSO Dynamics

Dietmar Dommenget[1], Sabine Haase[2], Tobias Bayr[2] and Claudia Frauen[1]

1: School of Mathematical Sciences, Monash University, Clayton, Australia
2: GEOMAR Helmholtz Centre for Ocean Research, Kiel, Germany

submitted to Climate Dynamics, revised October 10, 2013

Abstract

In a recent study it was illustrated that the El Nino Southern Oscillation (ENSO) mode can exist in the absence of any ocean dynamics. This oscillating mode exists just due to the interaction between atmospheric heat fluxes and ocean heat capacity. The primary purpose of this study is to further explore these atmospheric Slab Ocean ENSO dynamics and therefore the role of positive atmospheric feedbacks in model simulations and observations.

The positive solar radiation feedback to SST, due to reduced cloud cover for anomalous warm SSTs, is the main positive feedback in the Slab Ocean El Nino dynamics. The strength of this positive cloud feedback is strongly related to the strength of the equatorial cold tongue. The combination of negative latent heat flux to the east and positive sensible heat flux to the west of positive anomalies leads to the westward propagation of the SST anomalies, which allows for oscillating behavior with a preferred period of 6-7 years.

Several indications are found that parts of these dynamics are indeed observed and simulated in other atmospheric or coupled general circulation models (AGCMs or CGCMs). The CMIP3 AGCM-slab ensemble of 13 different AGCM simulations shows unstable ocean-atmosphere interactions along the equatorial Pacific related to stronger cold tongues. In observations and in the CMIP3 and CMIP5 CGCM model ensemble the strength and sign of the cloud feedback is a function of the strength of the cold tongue. In summary, this indicates that the Slab Ocean El Nino dynamics are indeed a characteristic of the equatorial Pacific climate that is only dominant or significantly contributing to the ENSO dynamics if the SST cold tongue is sufficiently strong. In the observations this is only the case during strong La Nina conditions.

The presence of the Slab Ocean ENSO mode in observations and CGCM model simulations implies that the family of physical ENSO modes does have another member, which is entirely driven by atmospheric processes and does not need to have the same spatial pattern nor the same time scales as the main ENSO dynamics.

1. Introduction

The El Nino Southern Oscillation (ENSO) is the globally most dominant mode of coupled atmosphere-ocean variability on seasonal to interannual time scales. The interaction between ocean and atmosphere is in general described by the Bjerknes feedbacks between sea surface temperature (SST), zonal winds in the central equatorial Pacific and the thermocline depth along the equatorial Pacific. In the most common picture of ENSO the ocean dynamics are considered to be the driving force of the mode [Neelin et al., 1998]. The dominant effect of these dynamics can be summarized in the conceptual model of the Recharge-Discharge Oscillator of heat content in the upper equatorial Pacific [e.g. Jin, 1997].

The net atmospheric heat fluxes are in general considered to be strong negative feedbacks in the ENSO mode [Neelin et al., 1998, Sun et al., 2006 or Bellenger et al., 2013 here referred to as B13]. However, Sun et al. [2006] and B13 pointed out that many coupled general circulation model (CGCM) simulations largely underestimate important negative feedbacks from the atmospheric heat fluxes. In particular, the short wave radiation feedback due to the response in cloud cover to changes in the SST deviates from the observations [Guilyardi et al., 2009, Lloyd et al., 2009 and B13]. B13 found that the response of the short wave radiation (clouds) is strongly linked to the mean SST along the equatorial Pacific with stronger simulated mean cold tongues leading to a weaker negative short wave radiation feedback.

Dommenget [2010, hereafter as D10] described ENSO-kind of variability entirely forced by atmospheric heat fluxes integrated by the ocean mixed layer heat capacity. A similar result was also found by Clement et al. [2011]. This kind of ENSO variability does neither involve any ocean dynamics (similar to the 'SST mode' in Neelin et al., 1998) nor any of the Bjerknes feedbacks. The Slab Ocean ENSO described in D10 is entirely controlled by the coupling between SST and atmospheric net heat flux, i.e. the sum of short wave radiation, thermal radiation, latent and sensible heat flux.

These dynamics described in the ECHAM5 atmospheric general circulation model (AGCM) appear to be quite different from the dynamics observed. It opens up the questions:

- How can the atmospheric heat fluxes alone cause an oscillating behavior in SST variability on interannual time scales in the AGCM slab ocean simulation?
- To what extent is this finding a model artifact of the ECHAM5 AGCM or do these dynamics exist in other AGCMs and in the observations?
- To what extent are the atmospheric dynamics of CGCM simulations and observations similar to this Slab Ocean El Nino mode?

The aim of this study is to address these questions. This study will illustrate how the combination of a positive short wave feedback and out-of-phase latent and sensible heat fluxes can result in SST oscillations on interannual time scales. We will further demonstrate that these dynamics are not a unique feature of the ECHAM5 model, but are indeed present in other AGCMs and in the observations under some circumstances. It will also be illustrated that the atmospheric dynamics in some coupled general circulation models (CGCMs) are more similar to the Slab Ocean El Nino dynamics than they are to the observed dynamics.

The paper is organized as follows: the following section introduces the datasets, model simulations and methods used in this study. In the first analysis section we explore the characteristics of the Slab Ocean ENSO dynamics in AGCMs coupled to a Slab Ocean model. In Section 4 we take a closer look at the positive cloud feedbacks in observations and CGCM simulations, and in Section 5 we finish the analysis sections with a discussion of the atmospheric heat flux terms in CGCM simulations. The study is concluded with a summary and discussion section.

2. Data and Methods

In this study we use several different observational datasets, reanalysis and different model simulations. Observed SSTs are based on the HADISST dataset from 1870 to 2011 [Rayner et al., 2003]. Cloud cover observations from 1984 to 2002 are taken from the ISCCP dataset [Rossow and Schiffer, 1999]. The observed atmospheric heat flux components and the net heat flux from 1984 to 2002 are taken from the Woods Hole Oceanographic Institution (WHOI) dataset, also referred to as the OA Flux dataset [Yu et al., 2008]. We also use the NCEP reanalysis from 1950 to 2010 [Kalnay et al., 1996] for comparison. The mean equatorial Pacific thermocline depth, *h*, is estimated by the depth of the 20°C isotherm, Z_{20}, (interpolated from oceanic potential temperature data) is taken from the BMRC dataset [Smith, 1995]. For the analysis of the observations we used the time period 1984-2002 from all datasets, as this is the largest overlapping time period.

Several different model ensembles are analyzed in this study: The ensemble of the ECHAM5-slab simulations from D10 is a set of 24 simulations, each 50yrs long, with the ECHAM5 [Roeckner et al., 2003] AGCM coupled to a simple Slab Ocean model. The 24 simulations differ only in their mean SST climatologies, which were forced to mimic the mean SSTs of 24 simulations from the coupled model inter-comparison project (CMIP) phase 3; (see Table 1). The run forced towards the CNRM-CM3 SST climatology, which has a very strong cold tongue, is one of the runs with the most pronounced Slab Ocean El Nino variability. This run is continued for 1000yrs (referred to as ECHAM5-$slab_{ELNINO}$).

The 53 CGCM simulations analyzed in this study are taken from the CMIP phase 3 and 5 (CMIP3 and CMIP5) database 20th century control simulations [Meehl et al., 2007 and Taylor et al., 2012]. The model simulations are either taken from the pre-industrial or 20th century scenarios. To avoid artificial model drifts or anthropogenic climate trends, all model data has been linearly detrended. For a complete list of the CGCM simulations see Table 1 and 2. The database does not provide subsurface ocean temperatures (for defining the thermocline depth) or heat fluxes for all the model simulations. Therefore some of the analyses presented below are only based on a subset of all the models.

Further we analyzed an ensemble of 13 different AGCMs coupled to a simple Slab Ocean model taken from the CMIP3 database. We took all AGCM-slab simulations in the database that had a 20th century control run. All AGCM-slab simulations are at least 20yrs long (see Table 1) and all simulations are flux corrected towards the observed mean SST climatology. The AGCM-slab simulations are the counterparts to some CMIP3 CGCM simulations; using the same AGCM, see Table 1.

All analyses presented here are based on monthly mean data, with the anomalies defined for each data set or model simulation individually relative to the data or models mean seasonal climatology. For the analysis of the heat flux or other forcing components contributions to the SST dynamics in the CMIP3 CGCM simulations we compare the auto-correlation of the SST, C_{SST}, and the cross-correlation of the SST with the SST tendencies, C_{dSSTdt}, (as shown in Fig. 1 for instance) with the cross-correlation of different forcing terms with the SST (red line in Fig. 1 for the net heat flux for instance). We quantify the similarity in these curves by computing the correlation between the Fisher z-transformed curves from lag -1 to 1 on the normalized x-axis. The normalization of the x-axis for all models is done by the oscillation period of each model, which is defined by the lag-time of the first local minima in the C_{SST} function of each model multiplied by two. We further weight the correlation estimated by an exponential-function decaying with |lag| to incorporate the exponentially decaying nature of C_{SST}. We can therefore estimate the similarity between forcings and C_{SST} or C_{dSSTdt} in all model simulations and observations independent of the individual ENSO period of each dataset and focusing on the ENSO phases between 0 and +/-180 degrees.
In this approach we can identify forcing terms as local feedbacks if they correlate with C_{SST}. With positive correlations indicating positive feedbacks and vice versa. Forcing terms that correlate with C_{dSSTdt} are out-of-phase feedbacks that drive the evolution of the SST. Again positive correlations indicate positive out-of-phase feedbacks that drive the evolution of the SST and vice versa.
We note here that our approach of comparing tendencies with forcing terms on the basis of correlations is only a qualitative evaluation of the relationships, which is motivated by the good description of the slab ocean El Nino mode in the ECHAM5-slab$_{ELNINO}$ simulation with this approach. It is not a quantitative heat budget analysis and can only give a first order indication of the relative role of different forcing terms.
The correlation between monthly mean SST and cloud cover anomalies as function of the mean SST is computed by first sorting the data into SST intervals according to the mean SST in the NINO3 region (150^{o}W to 90^{o}W / 5^{o}S to 5^{o}N) or the mean meridional SST gradient between the NINO3 region minus the mean of the regions 5^o to the north and south. Then anomalies of SST and cloud cover for each data set (e.g. models or observations) for each SST interval are computed relative to the intervals means. The correlation values are then computed based on the anomalies relative to the SST intervals means.

3. The Slab Ocean El Nino Dynamics

In this first analysis section we will layout in detail how the different heat flux components in the ECHAM5-slab$_{ELNINO}$ simulation respond to SST variations and how these interactions lead to the increased interannual oscillation of the Slab Ocean El Nino. We will summarize the essence of the interactions in a simple stochastic toy model. It is further illustrated how the strength of the SST variability depends on the mean SST climatology in the ensemble of the ECHAM5-slab simulations. In the second part of this section we will look for evidence of the Slab Ocean El Nino characteristics in other slab ocean AGCM simulations from the CMIP3 database.

The Slab Ocean El Nino dynamics are substantially different from what we know about the dynamics that control the ENSO mode. This can best be illustrated by comparing the SST tendency equations of the Slab Ocean model with the simple Recharge Oscillator model of Jin [1997]. The Slab Ocean SST tendencies are entirely controlled by the net atmospheric heat fluxes, F_{atmos}:

$$\frac{dSST}{dt} = F_{atmos} + Q_{clim} \qquad [1]$$

The flux corrections, Q_{clim}, control the mean SST climatology. They are state independent and therefore do not directly affect the evolution of SST anomalies. However, by influencing the mean SST they indirectly control the atmospheric response to the SST.

The Recharge Oscillator model as formulated by Burgers et al. [2005] is based on two coupled tendency equations between the anomalous NINO3 SST, T, and the anomalous mean equatorial Pacific thermocline depth, h. In the study of Frauen and Dommenget [2010] they are driven by atmospheric wind stress over the central Pacific region (160E-140W, 6S-6N), τ, and net atmospheric heat flux over the NINO3 region, F_{atmos}, from the full complexity atmospheric general circulation model ECHAM5 leading to the following two equations:

$$\frac{dT}{dt} = a_{11O}T + a_{12}h + c_{\tau A}\tau + \frac{1}{mc}F_{atmos} \qquad [2]$$

$$\frac{dh}{dt} = a_{21O}T + a_{22}h + c_{\tau O}\tau \qquad [3]$$

Details of the model parameters and how they are derived are given in Frauen and Dommenget [2010]. In the following we will refer to this model as RECHOZ.

The different nature of the Slab Ocean model and the Recharge Oscillator and how they relate to the observed behavior can best be illustrated on the basis of the cross-correlations at different lag/lead times between NINO3 SST anomalies, their tendencies, F_{atmos} and h, see Fig. 1. First of all, we can note that in all three cases the auto-correlation of the SST goes to significant negative values, peaking as defined at the normalized lag of 0.5, which indicates oscillating behavior in all three data sets. The ECHAM5-slab$_{ELNINO}$ simulation shows some unusual behavior with the lag 1 correlation being larger in amplitude than the lag 0.5 correlation (Fig. 1b), which reflects some non-linear behavior, which was also shown in D10. More importantly, in the ECHAM5-slab$_{ELNINO}$ simulation (Fig. 1b) we can also see that the cross-correlation between SST and the SST-tendencies, C_{dSSTdt}, is identical to the cross-correlation between SST and F_{atmos}, C_{atmos}. This illustrates that the SST anomalies in the ECHAM5-slab$_{ELNINO}$ simulation are by construction caused by F_{atmos} (eq. [1]). In contrast we see in Fig. 1a that the observed C_{atmos} is different. Here F_{atmos} is mostly opposing (acting against) the SST-tendencies, highlighting that the SST-tendencies are not caused by F_{atmos}.

The cross-correlation between observed NINO3 SST and Z_{20} (an estimate of h) is similar to C_{dSSTdt}, indicating that the Z_{20} anomalies cause the SST anomalies. This is nearly identical to the characteristics of the RECHOZ model (Fig. 1c). It is important to note here that the ECHAM5-slab$_{ELNINO}$ and the RECHOZ model simulations have the identical atmosphere model, but different SST tendencies (eqs. [1] and [2]) and different mean SST climatologies. The different mean SST can cause different atmospheric responses to the same SST anomalies in the two models.

To better understand the dynamics in the ECHAM5-slab$_{ELNINO}$ model we need to look at the four components of the net atmospheric heat flux, F_{atmos}:

$$F_{atmos} = F_{solar} + F_{thermal} + F_{latent} + F_{sense} \qquad [4]$$

The absorbed solar radiation, F_{solar}, the net thermal radiation, $F_{thermal}$, the latent heat loss, F_{latent}, and the turbulent sensible heat flux F_{sense}, make up the net atmospheric heat fluxes, F_{atmos}. All fluxes are defined to be positive downward, i.e. positive heat fluxes warm the ocean. In Fig. 2 it is illustrated how the four components of F_{atmos} cross-correlate to the SST and its tendencies in the ECHAM5-slab$_{ELNINO}$ simulation and in observations. In the ECHAM5-slab$_{ELNINO}$ simulation F_{solar} correlates with the SST and F_{sense} correlates best with the SST tendencies. The $F_{thermal}$ and F_{latent} heat fluxes are both anti-correlated with the SST. So in this model the driving forces are on average the F_{solar} and F_{sense}, whereas $F_{thermal}$ and F_{latent} are on average opposing the SST and therefore damp the SST.

This relation between the heat flux components and the SST is quite different in the observations. Here, most heat flux components are in average opposing the SST, which corresponds to a net damping of the SST. This is similar for the NCEP heat flux terms (not shown), but the thermal radiation is more closely related to the SST auto-correlation than to the SST-tendencies.

We can further explore the relative importance of the heat flux components in the ECHAM5-slab$_{ELNINO}$ simulation by the lag/lead regressions along the equatorial Pacific in a Hoevmoeller diagram (Fig. 3) and for lag=0 (Fig. 4). A few important characteristics can be pointed out here:

- The El Nino mode in the ECHAM5-slab$_{ELNINO}$ has a characteristic east-to-west propagation (Fig. 3a), which is a key element of the oscillating nature in this model with a period of about 6-7 yrs [D10].
- The most dominant driver of all four components is F_{solar}. Since anomalous F_{solar} can only be caused by variations in the cloud cover, we can conclude that the main driver is a positive cloud feedback. Reduced cloud cover leads to increased F_{solar} which amplifies the existing SST anomalies [D10].
- F_{latent} contributes to the build up of the SST anomalies, in particular in the central and western Pacific. It is also the main component that leads to the decay and westward propagation of the eastern edge of the SST anomalies [D10].
- In the ECHAM5-slab$_{ELNINO}$ simulation the strong cold tongue creates meridional temperature gradients, which together with converging winds for positive SST anomalies can lead to small but relevant positive F_{sense} by heat advection. It is interesting to note, that despite its very small amplitude, the F_{sense} is one of the main forcings for the SST evolution in the east to west propagation, in particular in the central and western Pacific (see Fig. 4). This indicates that F_{sense} could have a steering control on the SST evolution: It provides a small tendency for the westward propagation of the SST anomalies at the western edge of the SST anomaly.

In summary, we find that the most important element in the atmospheric heat flux forcing is a positive cloud feedback and the combination of F_{sense} and F_{latent} is important in the east-to-west propagation. This propagation along the equator is causing the preferred time scale oscillation in the ECHAM5-slab$_{ELNINO}$.

A simple toy model can illustrate the nature of the oscillating behavior in the ECHAM5-slab$_{ELNINO}$ simulation and the important roles that the positive feedback from F_{solar} and the equatorial out-of-phase feedbacks play:

$$\gamma \frac{dT(x_k,t)}{dt} = c_{local} \cdot T(x_k,t) + \sum_{i=1}^{8} c_{remote}(x_i,x_k) \cdot T(x_i,t) + \xi(x_k,t) \qquad [5]$$

In this simple stochastic model of the SST variability (anomalies) of 8 points along the equator, $T(x_k,t)$, the tendencies of T times the heat capacity, γ, are forced by three terms: a local damping with $c_{local} = -0.5 \, W/m^2K$, a remote forcing from all other locations along the equator proportional to the strength of c_{remote}, and a white noise forcing, ξ, with a standard deviation of 25W/m^2. This simple linear model captures the essence of the heat flux interactions along the equator in the ECHAM5-slab$_{ELNINO}$ simulation as illustrated in Figs. 3 and 4. It does not capture the non-linear aspects of the ECHAM5-slab$_{ELNINO}$ simulation as shown in D10 or indicated by Fig. 1b.

The strength of the local damping is determined by the sum of all heat fluxes, but is dominated by F_{solar} in the ECHAM5-slab$_{ELNINO}$ simulation. c_{remote} is a function of location as can be seen in Fig. 4 relative to the NINO3 .4 region (190^{o}E to 240^{o}E; 5^{o}S to 5^{o}N). The forcing is positive for locations to the west with amplitude of about +1 to +3W/m^2/K and negative for locations to the east with amplitude about -2 to -4W/m^2/K if T is positive in the NINO3 .4 region. A comparison of Fig. 3b, c and g and Fig. 4 shows that F_{sense} plays an important role in the remote forcing term to the west. We integrated this model for 10^4 years with a daily time step.

In Figure 5 the power spectra of the ECHAM5-slab$_{ELNINO}$ simulation and the toy model are shown. We can see that both models show similar spectra with a peak at around 7yrs. To mimic the ECHAM5-slab simulations that do not have strong El Nino variability (D10) we can assume that the remote forcing is missing (second term RHS in eq. [5]) and that due to the missing positive cloud feedback the local damping is much stronger ($c_{local} = -2.5 \, W/m^2K$). The result of this model is shown as the red line in Fig. 5b. The dark blue and green lines in Fig. 5b are the results of the model without the remote forcing or with a stronger negative feedback only. In the light blue line we have not considered the F_{sense} term in the remote forcing. We can see that this has a significant impact on the preferred period. In summary the toy model highlights the important role of the positive cloud feedbacks to increase the low-frequency variability and it highlights the role of the propagation (remote forcing) in creating the oscillation. In the latter case the out-of-phase feedbacks of F_{sense} and F_{latent} are important even though they are small in amplitude. They both have a steering control of the propagation. This weak steering control is only capable in producing an oscillation if the effective sum of all local feedbacks is weak (near zero) due to the positive cloud feedback.

We now need to address the question: are the ECHAM5 AGCM feedbacks unique to the ECHAM5-slab model simulations or do they exist in other model simulations and even in the observations.

In the set of 24 different ECHAM5-slab simulations the positive cloud feedback is strongly controlled by the mean SST climatology [D10]. Only the simulations that have much stronger than observed equatorial cold tongues, have the El Nino kind of variability in the ECHAM5-slab runs, see Fig. 6. Thus even in the ECHAM5-slab ensemble we do not see the Slab Ocean El Nino mode for current mean SST conditions. Figure 7a shows the spatial structure of the mean SST spread in the ECHAM5-slab simulations. It clearly points out the large uncertainty in the control SST in the NINO3 region. In order to illustrate that the different mean SST climatologies lead to different SST variability, we define Slab Ocean El Nino variability *ON* as those runs in the ECHAM5-slab ensemble with the mean meridional SST difference between the NINO3 region minus the mean of the regions 5° to the north and south smaller -1.8°C and the other runs as Slab Ocean El Nino mode *OFF*. This threshold roughly marks the meridional SST difference at which the SST variability in the ECHAM5-slab simulations appears to be increasing beyond the background variability level of about 0.5°C (see Fig. 6b). The average SST of those models with the Slab Ocean El Nino variability *ON* shows the signature of the too strong cold tongue bias (Fig. 7c). This is to some degree forced by the selection of the ON and OFF ensemble. More importantly, the ratio in SST standard deviation of the models with a strong cold tongue relative to all the models with a weak cold tongue is strongly enhanced in the NINO3 region (Fig. 7e).

We can further illustrate that the patterns of variability in the tropical Pacific are quite different between the ECHAM5-slab runs with El Nino ON or OFF; see Fig. 8. In the El Nino ON ensemble the leading EOF-1 has the equatorial El Nino pattern structure, whereas the EOF-1 of the El Nino OFF ensemble is missing the equatorial signature. A good way to quantify the differences in the leading modes of variability between the two datasets is by rotating the leading modes towards the pattern that maximizes the explained variance differences between the two datasets according to the methods of Dommenget [2007] and Bayr and Dommenget [2013]. The pattern that is most dominant in the El Nino ON ensemble, but missing in the El Nino OFF ensemble, is the equatorial pattern DEOF-1 (Fig. 8e, with an explained variance of 37% in El Nino ON and 4% in El Nino OFF), which is similar to the EOF-1 of the El Nino ON ensemble.

We can now look at other Slab Ocean model simulations to explore the possibility that the Slab Ocean El Nino mode exists in other models as well. We therefore analyze 13 control Slab Ocean simulations of the 20th century from the CMIP3 database; see Table 1. It needs to be noted here that the CMIP ensemble has some important differences relative to the ECHAM5-slab ensemble: First of all the CMIP3 slab simulations are relatively short, with most of them just 20-50yrs long (see Table 1). Further, the Slab Ocean simulations of the CMIP ensemble are all flux corrected to fit to observed SST, whereas the ECHAM5-slab ensemble is forced to mimic the CMIP3 coupled model SST climatologies [D10]. Subsequently the cold tongues in the CMIP3 slab ensemble are not as pronounced as in the ECHAM5-slab ensemble; see Fig. 6b. In order to capture at

least two models with a relatively strong cold tongue (MRI_CGCM2.3.2 and ncar_ccsm3_0), we select CMIP3 slab ensemble El Nino ON with a threshold of -1.5°C instead of -1.8°C for the ECHAM5-slab ensemble.
For the signatures of the Slab Ocean El Nino mode as presented in Fig. 6, 7 and 8 we can make the following findings for the CMIP3 slab ensemble:

- The CMIP3 slab simulations show an enhanced spread in the mean SST climatologies along the eastern equatorial Pacific (Fig. 7b) comparable to the CMIP CGCM models (not shown) and the ECHAM5-slab simulations (Fig. 7a), even though they are all forced by flux corrections towards the observed SST climatology. This suggests that the CMIP3 slab simulations have some unstable ocean-atmosphere interaction that must be related to atmospheric feedbacks, since no ocean feedbacks exist in these simulations.
- Similar to the ECHAM5-slab ensemble the CMIP3 slab simulations with the stronger SST variability have also a stronger mean cold tongue (Fig. 7c and d).
- In turn, the CMIP3 slab simulations with a stronger mean cold tongue (MRI_CGCM2.3.2 and ncar_ccsm3_0) have an enhanced ratio in SST standard deviation along the equatorial band relative to all the models with a weak cold tongue, which is focused almost entirely onto the NINO3 region (Fig. 7f). It needs to be noted here that the mean SSTs in these CMIP3 slab simulations are not directly related to the mean SSTs in the coupled CGCM simulations using the same atmosphere model. In the coupled simulations the mean SST climatology is a result of coupled dynamics. In the CMIP3 slab simulations the mean SST is forced towards observations by flux corrections. Limitations in the estimation of the flux corrections for CMIP3 slab simulations cause differences in the mean SST.
- The CMIP3 slab El Nino ON simulations have an equatorial El Nino like variability pattern that is missing in the other El Nino OFF simulations (Fig. 8b, d and f).
- However, it is not yet clear if any of the CMIP3 models does have the oscillating Slab Ocean El Nino mode. It needs to be noted that the CMIP3 slab simulations are too short to note oscillations in these runs. More importantly, none of the CMIP3 simulations is in the range of very strong cold tongues, in which the ECHAM5-slab simulations with strong El Nino like variability are (below -1.8°C in Fig. 6b). Again this is related to the fact that the CMIP3 models are forced towards an observed mean SST, which does not allow the strong cold tongue, whereas the ECHAM5-slab simulations are forced towards the CMIP3 CGCM models mean SSTs, which do have very strong cold tongues.

In summary, we find that the CMIP3 slab simulations agree relatively well with the ECHAM5-slab simulations in their Slab Ocean El Nino characteristics. Indeed, it seems possible that most other atmospheric GCMs are capable of producing the Slab Ocean El Nino if forced into a strong mean SST cold tongue condition.

4. Positive Cloud Feedbacks

In the previous section we have shown that a positive cloud feedback is one of the main elements of the Slab Ocean El Nino mode. We now like to further explore how this positive cloud feedback depends on the mean SST and if it exists in observations and other models as well.

In Figure 9 we show the correlation between SST and cloud cover for the tropical Pacific domain. In the ECHAM5-slab ensemble we defined SST anomalies relative to the climatological SST mean of each of the 24 simulations and then combined several simulations to one ensemble. In the 18 ECHAM5-slab simulations with the meridional mean SST difference (Fig. 6b) larger than -1.8^{o}C (hereafter “El Nino mode OFF” ensemble) the correlation between SST and cloud cover is positive throughout most of the domain (Fig. 9a). It is strongest in the off equatorial and western Pacific. On the other hand, for the El Nino mode ON ensemble the correlation between SST and cloud cover is negative along the equatorial and eastern Pacific (Fig. 9b). This negative correlation is consistent with the positive cloud feedback and positive correlation between F_{solar} and NINO3 SST (Fig. 2b): the warmer the SST the smaller the cloud cover and subsequently the larger the anomalous F_{solar}. The difference between the “El Nino mode ON” and “El Nino mode OFF” ensembles (Fig. 9c) is strongly negative along the central equatorial Pacific, clearly highlighting that the positive cloud feedback is a prominent signature of the ECHAM5-slab “El Nino mode ON” ensemble.

Since the two ensembles are selected by the mean SST difference between the equatorial cold tongue and the higher latitudes, it seems reasonable to assume that the positive cloud feedback is effectively a function of the mean SST. Figure 10 quantifies this non-linear relationship by the strength of the correlation between SST and cloud cover as a function of the mean SST (see data and methods section for details). Overall, the correlation between SST and cloud cover is clearly a function of the mean SST (Fig. 10b). For positive or near zero meridional mean SST differences (weak or no cold tongue) the correlation between SST and cloud cover is positive, but for negative meridional mean SST differences (normal or strong cold tongue) the correlation between SST and cloud cover is more negative. This relationship is also present in the mean NINO3 SST (Fig. 10a), but is not as clear as for the meridional mean SST differences and it also apparently breaks down for the very extreme NINO3 mean SST values (18^{o}C or 28^{o}C).

We now repeat the above analysis for the observations. We have to keep in mind that the mean SST in the ECHAM5-slab simulations varies over a much wider range than it is observed. In the observations the meridional mean SST difference ranges between -2^{o}C to 0^{o}C, but in the ECHAM5-slab simulations it ranges from -6^{o}C to 1^{o}C. Similarly the mean NINO3 SST in the ECHAM5-slab simulations reaches much lower (<23^{o}C) values than observed (compare Fig. 10a and c). However, despite the fact that the observed SST mean values are confined on a much warmer and narrower range, we find a qualitatively similar, but quantitatively more pronounced behavior in the observations. The correlation between SST and cloud cover is more negative if the cold tongue is stronger and it is more positive if the mean cold tongue is weaker (Fig. 10c and d). This is also consistent with the result of Fig. 9d-f. Here we find that overall the correlation between SST and cloud cover is positive, but for the coldest 25% of all monthly mean NINO3 SSTs the correlation is more negative, in particular in the central and eastern Pacific equatorial region. Thus in time periods of relatively strong cold tongues, typically in August to October or during La Nina conditions, the normally negative cloud feedback turns into a weak positive feedback.

5. Dynamics of Coupled GCM Simulations

In the previous section we illustrated that some of the ECHAM5-slab El Nino mode characteristics exist not only in other AGCMs coupled to Slab Ocean models, but that the positive cloud feedback exists in the observations as well. We now explore the CMIP CGCM model ensemble to search for evidence of the Slab Ocean El Nino mode characteristics in these simulations.

For the analysis of the cloud feedback relationship with the mean SST (Figs. 9 and 10) we treat all the models of the CMIP ensemble as one large dataset. Anomalies are computed relative to the mean SST of each model. Figures 9 and 10 illustrate that the CMIP CGCM model ensemble has qualitatively the same mean SST depending cloud feedback relationship as it was found in ECHAM5-slab simulations and observations. The cloud feedback is more negative for data points throughout all the models, where the absolute SST is relatively low (the lowest 10% of all data; Fig. 9h). As in the observations and the ECHAM5-slab simulation the correlations are shifted to negative values in the central Pacific along the equator (Fig. 9i). However, the amplitude of this shift is much weaker than in observations or the ECHAM5-slab simulations. The non-linearity in the cloud feedback as a function of the mean SST in the NINO3 region appears to exist in the CMIP CGCMs as well (Fig. 10 e and f). Again, this relationship is weaker than observed and it appears to break down for the most extreme NINO3 mean SST cases (Fig. 10e).

We can repeat the analysis of Fig. 9 and 10 for each of the CMIP CGCM simulations individually. Basically all models show a shift towards a positive cloud feedback (less clouds for positive SST anomalies, i.e. negative correlation) for relative strong cold tongues. Only the models, which already have a relatively strong positive cloud feedback, do not show this shift towards a stronger positive cloud feedback for relative strong cold tongues.

The results for the CMIP models above are qualitatively in agreement with the study of B13. They also find that the cloud feedbacks are a function of the mean SST and in particular that the positive cloud feedbacks are more likely in colder mean SSTs and in the cold season (Aug. to Oct.).

We now like to further explore if the NINO3 SST dynamics or tendencies of the individual models of the CMIP CGCM ensemble follow the Recharge Oscillator model, as observed or in the RECHOZ model (Fig. 1a and c), or whether they show indications of the Slab Ocean El Nino mode. We base this analysis on a qualitative comparison (correlation) of forcing terms with C_{SST} or C_{dSSTdt} (as shown in Figs. 1 and 2 for the observations and ECHAM5-slab$_{ELNINO}$). In Fig. 1b, for instance, we find that C_{dSSTdt} (dashed line) is identical to the cross-correlation function of the SST with the net heat flux, $C_{netheat}$, (red line). This can be quantified by a lag-weighted correlation between the two curves (see data and methods sections for details), which is 1.0 in this case. Similarly the correlation values can be computed for each of the forcing components. We note here again that our approach is only a qualitative evaluation of the relationships. It is not a quantitative heat budget analysis and can only give a first order indication of the relative role of different forcing terms.

Figure 11 shows the correlations for all six different forcing components for the observations, NCEP, ECHAM5-slab$_{ELNINO}$, RECHOZ and all CMIP CGCM simulations. Starting with the ECHAM5-slab$_{ELNINO}$ simulation to illustrate the meaning of the correlation values, we can see that $C_{netheat}$ has a correlation of 1.0 with C_{dSSTdt}, as mentioned before (Fig. 11b). It illustrates that the SST tendencies are caused by the net heat flux. C_{sense} (the cross-correlation function between SST and F_{sense}) is highly correlated (0.85) with C_{dSSTdt}, but has only a weak correlation with C_{SST}, see Fig. 11f. This quantifies what we can see in Fig. 2b by comparing C_{sense} (green line) with C_{SST} (dashed line). We further find that C_{solar} (the cross-correlation function between SST and F_{solar}) is highly correlated (0.6) with C_{SST}, but has only a weak correlation with C_{dSSTdt} and both C_{latent} (the cross-correlation function between SST and F_{latent}) and $C_{thermal}$ (the cross-correlation function between SST and $F_{thermal}$) are negatively correlated with C_{SST}, but have only weak correlations with C_{dSSTdt} (Fig. 11 d and e).

For the observations and for the RECHOZ simulation the relationships are quite different: $C_{netheat}$ is anti-correlated with C_{SST} and has no significant correlation with C_{dSSTdt}. In both, the observations and the RECHOZ simulation the cross-correlation of the thermocline depth and the SST, C_{Z20}, has the largest positive correlation with C_{dSSTdt}. The NCEP reanalysis heat fluxes appear to be similar to the observed, but the absolute values of the correlations with C_{SST} are larger than in any other data set. This may indicate some limitations in the NCEP reanalysis heat fluxes.

The main features of the ensemble of the CMIP models can be summarized to the following points:

- All models have a strong positive correlation of the C_{Z20} with C_{dSSTdt}, consistent with what we expect from the recharge oscillator model. The agreement between the models in this relationship is relatively high.
- Most models have no significant correlation of $C_{netheat}$ with C_{dSSTdt} and mostly negative correlations with C_{SST}, suggesting that atmospheric heat flux forcings are mostly damping the SST.
- All models strongly agree on a negative correlation between C_{latent} and C_{SST}, suggesting that the local latent heating is damping the SST variability in all models.
- The models show a wider spread in the heat flux components F_{solar}, $F_{thermal}$ and F_{sense} relation to both C_{SST} and C_{dSSTdt} than in F_{atmos}. This suggests that the spread in the individual components is compensating each other when combined to the total F_{atmos}. In each of these components they seem to cluster into two groups. Here F_{solar} and $F_{thermal}$, have largely opposite behavior, highlighting the compensating effect of thermal and solar radiation due to cloud cover variations.
- The larger group of models has a positive correlation between C_{solar} and C_{SST} or C_{dSSTdt}, which is opposite of what is observed and is more similar to the ECHAM5-slab. For most models $C_{thermal}$ has the opposite correlation of what C_{solar} has, supporting the mostly opposite thermal radiation cloud feedback.

- The correlation with C_{sense} clusters in two groups: one with negative correlation to C_{SST}, as observed. The other with positive correlation to C_{SST}. Positive correlations with C_{dSSTdt}, as in the ECHAM5-slab, are mostly not simulated.

In summary, we can state that most of the models show very little indications that positive atmospheric forcing feedbacks, such as in the Slab Ocean El Nino, control the SST dynamics. Nearly all models clearly fit to the concept of the recharge oscillator model. However, many models do show positive cloud and sensible heat flux feedbacks.

We can summarize this analysis by computing the distance (root-mean-square error) of the correlation values as shown in Fig. 11b-f for all the CMIP simulations, observations, NCEP, RECHOZ and the ECHAM5-slab$_{ELNINO}$ simulation relative to the observation and the ECHAM5-slab$_{ELNINO}$ simulation; see Fig. 12. The following points can be made from this figure:

- We can see that most CMIP simulations are closer to the observed atmospheric heat flux feedbacks than they are to the ECHAM5-slab$_{ELNINO}$ simulation (they are above the diagonal in Fig. 12).
- The models closest to the observed heat flux versus SST relationships (CGCM3.1(T63), GISS–AOM, ACCESS1, CCSM4, GFDL–ESM2M, NorESM1–ME) have all negative cloud and sensible heat flux feedbacks and they all do not have a strong cold tongue relative to the off equatorial regions. Most of them have no east-to-west propagation of the SST anomalies (not shown), but some do have indications of that (GISS-AOM and NorESM1–ME). B13 ranked these models in the heat flux and short wave feedbacks relatively high as well.
- The models that in terms of the heat flux versus SST relationships are closest to the ECHAM5-slab$_{ELNINO}$ simulation and most remote from the observations (BCCR–BCM2.0, CNRM–CM3, GISS–EH, INM–CM3.0, BCC–CSM1–1, CSIRO–Mk3–6–0, INMCM4 all have positive cloud and sensible heat flux feedbacks, SST anomalies propagating from the east to the west (only weakly in BCC–CSM1–1) and stronger cold tongues than the CMIP ensemble mean. All these features are consistent with the Slab Ocean ENSO mode in the ECHAM5-slab ensemble. B13 ranked these models in the heat flux and short wave feedbacks relatively low as well.
- The CMIP3 model BCCR–BCM2.0 (grey 1 in Fig. 12) shows the strongest indications that positive atmospheric forcing feedbacks control the evolution of the SST. Fig. 13 shows some statistics of the BCCR–BCM2.0 simulation, which again shows remarkable similarities in the heat flux forcings with the ECHAM5-slab$_{ELNINO}$ simulation (Figs. 1-3 and 7). This model has also a very strong cold tongue and SST anomalies propagating from the east to the west.

6. Summary and discussion

The primary purpose of this study was to further explore the Slab Ocean El Nino dynamics and therefore the role of atmospheric positive feedbacks controlling the dynamical evolution of the SST in the ENSO mode. We essentially addressed three questions, for which we summarize the answers below:

Firstly, how can the atmospheric heat fluxes alone cause an oscillating behavior on interannual time scales in the AGCM slab ocean simulation? The Slab Ocean El Nino dynamics are summarized in a simple toy model in eq. [5], whose main features are as follows:

- A strong mean cold tongue SST supports a relatively strong positive cloud feedback, which allows for unstable interannual SST variability along the equatorial Pacific.
- The combination of latent and sensible heat fluxes leads to the propagation of the SST anomalies from the east to the west. Even though these forcings are weak, they can lead to substantial interannual oscillations in the presence of weak overall local feedbacks due to the strong positive cloud feedback.

Secondly, to what extent is this finding a model artifact of the ECHAM5 AGCM or do these dynamics exist in other AGCMs and in the observations? We could demonstrate that the Slab Ocean El Nino dynamics are not a model artifact of the ECHAM5 AGCM. The following we found:

- The CMIP3 AGCM-slab ensemble of 13 different AGCM simulations shows enhanced spread in the mean SST climatology along the equatorial Pacific, despite the application of flux corrections towards the observed SST climatologies. This suggests that the coupled system of the AGCM-slabs of this model ensemble has unstable ocean-atmosphere interaction, as in the ECHAM5-slab ensemble. This unstable interaction allows for large SST variability for a given forcing.
- The simulations of the CMIP3 AGCM-slab ensemble with the strongest cold tongues have the strongest SST variability and the leading mode of variability along the equatorial Pacific, consistent with the ECHAM5-slab ensemble.
- In observations and in the CMIP CGCM model ensemble the strength and sign of the cloud feedback is a function of the mean SST in the equatorial Pacific, which is qualitatively consistent with the ECHAM5-slab ensemble. This modeling result is largely consistent with B13. In the observations a positive cloud feedback under current climatic conditions may only exist during strong La Nina conditions, supporting strong cold tongues.

In summary, this indicates that the presence of the Slab Ocean El Nino dynamics is to first order not related to some model characteristics (e.g. cloud parameterizations), but is indeed a characteristic of the equatorial Pacific climate that is only dominant or significantly contributing to the ENSO dynamics if the SST cold tongue is sufficiently strong. In the observations this is usually not the case, but during the seasons with stronger cold tongues or strong La Nina conditions it is.

Finally, to what extent are the atmospheric dynamics (heat flux relation to SST) of CGCM simulations and observations similar to this Slab Ocean El Nino mode? We chose a qualitative comparison of SST tendencies with forcing terms to highlight possible driving mechanisms. It has to be noted here that this is not a quantitative heat budget analysis. It therefore only provides indications of the relative role of atmospheric heat flux forcing terms or feedbacks in the ENSO dynamics. We find the following main qualitative behavior:

- Most models follow the recharge oscillator mechanism with Z_{20} leading the SST tendencies and net atmospheric heat fluxes damping the SST variability. This is consistent with the mean behavior in the observations. However, some models have the net atmospheric heat fluxes as a significant driver of the SST dynamics.

- Seven (BCCR–BCM2.0, CNRM–CM3, GISS–EH, INM–CM3.0, BCC–CSM1–1, CSIRO–Mk3–6–0 and INMCM4) out of the 49 model simulations appear to have atmospheric dynamics (surface heat fluxes) that are quantitatively closer to the Slab Ocean ENSO dynamics than they are to the observed atmospheric dynamics. For these models it has to be assumed that the Slab Ocean ENSO dynamics play a significant part in the overall ENSO dynamics of the models.
- The models that are closest to the observed atmospheric dynamics as analyzed in this study are: CGCM3.1(T63), GISS–AOM, ACCESS1, CCSM4, GFDL–ESM2M and NorESM1–ME. These models appear to be most realistic in the atmospheric heat flux feedbacks in the ENSO cycle. However, it needs to be noted here that this does not imply that these models are overall most realistic in their ENSO dynamics, as neither the oceanic feedbacks nor the overall ENSO dynamics have been analyzed in this study.

The results have some implications for ENSO dynamics as such and for CGCM model simulations. First of all it is clear from this analysis that ENSO modes can have different driving mechanisms, which are to some part caused by atmospheric feedbacks. The different mechanisms of variability do not need to have the same spatial pattern nor do they need to have the same time scales. Thus, ENSO in model simulations can follow different mechanisms. This may to some extend explain why state of the art climate models still differ substantially in their characteristics of ENSO at present day climate and in future climate change projections [Guilyardi et al., 2009, Collins et al., 2010].

In the development of CGCM simulations the development team is often faced with the problem that the tropical Pacific coupled climate system needs to be '*tuned*' to the observed climate by changing parameters in not well defined parameterizations. In previous developments the strength of the ENSO mode may have been an indicator of a good representation of the tropical Pacific coupled ocean-atmosphere dynamics. However, the results of this study and also that of B13 suggest that the overall ENSO statistics in terms of strength, pattern or period are not sufficient to determine a realistic ENSO behavior. The development of CGCM simulations needs to consider the right dynamics controlling the ENSO mode. As such, analysis of the atmospheric feedbacks as presented in this study should contribute to determine realistic ENSO simulations. A proper estimation of the skill in simulating realistic ENSO-dynamics should be based on multi-variate indices of the feedback/forcing terms controlling the ENSO dynamics, such as the terms of the Bjerknes (BJ) stability index [Jin et al., 2006] and an index of the atmospheric feedback such as presented in Fig. 11 and 12. In that atmospheric and oceanic processes should be discussed independent of each other, if possible.

Finally, it has to be noted that the work presented here may have some implications for the cloud feedback's contribution to the climate sensitivity to anthropogenic forcings. Cloud feedbacks, in particular over the tropical oceans, are one of the main sources of uncertainty in the climate sensitivity to anthropogenic forcings in CGCM simulations [Bony and Dufresne, 2005, Webb et al., 2006 and Williams and Webb, 2009]. We have illustrated here that the feedbacks of the clouds in the equatorial Pacific are strongly depending on the mean cold tongue SST. This difference in the feedbacks of the clouds can contribute to the overall uncertainty in the cloud feedbacks contribution to the climate sensitivity. Improving the ENSO dynamics, by improving the mean cold tongue SST bias and the unrealistic cloud feedbacks, will most likely reduce the uncertainties in the climate sensitivity to anthropogenic forcings by some (maybe small) amount.

Acknowledgements

We like to thank Gerrit Burgers, Eric Guilyardi and an anonymous referee for their constructive comments, which helped to improve this article substantially. This work was supported by the ARC Centre of Excellence for Climate System Science (Grant CE110001028) and the Deutsche Forschungsgemeinschaft (DFG) through project DO1038/5-1.

References

Bayr, T. and D. Dommenget, 2013: Comparing the spatial structure of variability in two datasets against each other on the basis of EOF modes. *Climate Dynamics***,** in press.

Bellenger, H., E. Guilyardi, J. Leloup, M. Lengaigne, and V. J., 2013: ENSO representation in climate models: from CMIP3 to CMIP5. *Climate Dynamics***,** in press.

Bony, S. and J. L. Dufresne, 2005: Marine boundary layer clouds at the heart of tropical cloud feedback uncertainties in climate models. *Geophysical Research Letters*, **32.**

Burgers, G., F. F. Jin, and G. J. van Oldenborgh, 2005: The simplest ENSO recharge oscillator. *Geophysical Research Letters*, **32,** -.

Clement, A., P. DiNezio, and C. Deser, 2011: Rethinking the Ocean's Role in the Southern Oscillation. *Journal of Climate*, **24,** 4056-4072.

Collins, M., S. I. An, W. J. Cai, A. Ganachaud, E. Guilyardi, F. F. Jin, M. Jochum, M. Lengaigne, S. Power, A. Timmermann, G. Vecchi, and A. Wittenberg, 2010: The impact of global warming on the tropical Pacific ocean and El Nino. *Nature Geoscience*, **3,** 391-397.

Dommenget, D., 2007: Evaluating EOF modes against a stochastic null hypothesis. *Climate Dynamics*, **28,** 517-531.

——, 2010: The slab ocean El Nino. *Geophysical Research Letters*, **37,** -.

Frauen, C. and D. Dommenget, 2010: El Nino and La Nina amplitude asymmetry caused by atmospheric feedbacks. *Geophysical Research Letters*, **37,** -.

Guilyardi, E., P. Braconnot, F. F. Jin, S. T. Kim, M. Kolasinski, T. Li, and I. Musat, 2009: Atmosphere Feedbacks during ENSO in a Coupled GCM with a Modified Atmospheric Convection Scheme. *Journal of Climate*, **22,** 5698-5718.

Guilyardi, E., A. Wittenberg, A. Fedorov, M. Collins, C. Z. Wang, A. Capotondi, G. J. van Oldenborgh, and T. Stockdale, 2009: Understanding El Nino in Ocean-Atmosphere General Circulation Models Progress and Challenges. *Bulletin of the American Meteorological Society*, **90,** 325-+.

Jin, F. F., 1997: An equatorial ocean recharge paradigm for ENSO .1. Conceptual model. *Journal of the Atmospheric Sciences*, **54,** 811-829.

Jin, F. F., S. T. Kim, and L. Bejarano, 2006: A coupled-stability index for ENSO. *Geophysical Research Letters*, **33**.

Kalnay, E., M. Kanamitsu, R. Kistler, W. Collins, D. Deaven, L. Gandin, M. Iredell, S. Saha, G. White, J. Woollen, Y. Zhu, M. Chelliah, W. Ebisuzaki, W. Higgins, J. Janowiak, K. C. Mo, C. Ropelewski, J. Wang, A. Leetmaa, R. Reynolds, R. Jenne, and D. Joseph, 1996: The NCEP/NCAR 40-year reanalysis project. *Bulletin of the American Meteorological Society*, **77,** 437-471.

Lloyd, J., E. Guilyardi, H. Weller, and J. Slingo, 2009: The role of atmosphere feedbacks during ENSO in the CMIP3 models. *Atmospheric Science Letters*, **10,** 170-176.

Meehl, G. A., C. Covey, T. Delworth, M. Latif, B. McAvaney, J. F. B. Mitchell, R. J. Stouffer, and K. E. Taylor, 2007: The WCRP CMIP3 multimodel dataset - A new era in climate change research. *Bulletin of the American Meteorological Society*, **88,** 1383-+.

Neelin, J. D., D. S. Battisti, A. C. Hirst, F. F. Jin, Y. Wakata, T. Yamagata, and S. E. Zebiak, 1998: ENSO theory. *Journal of Geophysical Research-Oceans*, **103,** 14261-14290.

Rayner, N. A., D. E. Parker, E. B. Horton, C. K. Folland, L. V. Alexander, D. P. Rowell, E. C. Kent, and A. Kaplan, 2003: Global analyses of sea surface temperature, sea ice, and night marine air temperature since the late nineteenth century. *Journal of Geophysical Research-Atmospheres*, **108,** -.

Roeckner, E., G. Bäuml, L. Bonaventura, R. Brokopf, M. Esch, M. Giorgetta, S. Hagemann, I. Kirchner, L. Kornblueh, E. Manzini, A. Rhodin, S. U., U. Schulzweida, and A. Tompkins, 2003: The atmospheric general circulation model ECHAM 5. Part I: Model description. *Reports of the Max-Planck-Institute for Meteorology*, **349**.

Rossow, W. B. and R. A. Schiffer, 1999: Advances in understanding clouds from ISCCP. *Bulletin of the American Meteorological Society*, **80,** 2261-2287.

Smith, N. R., 1995: An Improved System for Tropical Ocean Subsurface Temperature Analyses. *Journal of Atmospheric and Oceanic Technology*, **12,** 850-870.

Sun, D. Z., T. Zhang, C. Covey, S. A. Klein, W. D. Collins, J. J. Hack, J. T. Kiehl, G. A. Meehl, I. M. Held, and M. Suarez, 2006: Radiative and dynamical feedbacks over the equatorial cold tongue: Results from nine atmospheric GCMs. *Journal of Climate*, **19,** 4059-4074.

Taylor, K. E., R. J. Stouffer, and G. A. Meehl, 2012: An Overview of Cmip5 and the Experiment Design. *Bulletin of the American Meteorological Society*, **93,** 485-498.

Webb, M. J., C. A. Senior, D. M. H. Sexton, W. J. Ingram, K. D. Williams, M. A. Ringer, B. J. McAvaney, R. Colman, B. J. Soden, R. Gudgel, T. Knutson, S. Emori, T. Ogura, Y. Tsushima, N. Andronova, B. Li, I. Musat, S. Bony, and K. E. Taylor, 2006: On the contribution of local feedback mechanisms to the range of climate sensitivity in two GCM ensembles. *Climate Dynamics*, **27,** 17-38.

Williams, K. D. and M. J. Webb, 2009: A quantitative performance assessment of cloud regimes in climate models. *Climate Dynamics*, **33,** 141-157.

Yu, L., X. Jin, and R. A. Weller, 2008: Multidecade Global Flux Datasets from the Objectively Analyzed Air-sea Fluxes (OAFlux) Project: Latent and Sensible Heat Fluxes, Ocean Evaporation, and Related Surface Meteorological Variables. *Woods Hole Oceanographic Institution OAFlux Project Technical Report*, **OA-2008-01,** 64.

Figures

Figure 1.: Lag/lead auto- and cross-correlations with the NINO3 SST. Auto-correlation of the NINO3 SST (solid black line), cross-correlation with the NINO3 SST tendencies (dashed black line), with NINO3 F_{atmos}(red line) and tropical Pacific h (blue line). (a) for observations, (b) for the ECHAM5-slab$_{ELNINO}$ simulation and (c) for the RECHOZ simulation. The x-axis is normalized by the El Nino oscillation period of each dataset; see methods section for details. The numbers in the legends refer to the correlation values of the forcing curves with the SST and the SST tendency curves, as defined in the methods section.

Figure 2.: Lag/lead auto- and cross-correlations with the NINO3 SST, as in Fig. 1, but for cross-correlations with the heat flux components: F_{solar} (yellow), $F_{thermal}$ (red), $F_{sensible}$ (green) and F_{latent} (blue). All heat fluxes are defined positive downward. (a) for observations and (b) ECHAM5-slab$_{ELNINO}$. The two values in brackets are the correlations with SST autocorrelation and SST tendencies curves, respectively.

Figure 3.: Hoevmoeller diagrams along the equatorial (3°S to 3°N) Pacific of lag/lead regressions with the SST in the NINO3.4 region (170°W to 120°W / 5°S to 5°N) in the ECHAM5-slab$_{ELNINO}$ simulation. (a) Auto-regression in [K/K], (b) F_{atmos}, (c) the sum F_{solar} +$F_{thermal}$ +F_{latent}, (d) F_{solar}, (e) $F_{thermal}$, (f) F_{latent} and (g) F_{sense}. Values in (b)-(g) are in [W/m^2/K]. The y-axis is lag/lead month. The solid thick line in all panels is the 0.7 contour line from (a).

Figure 4.: Regressions of F_{atmos} and F_{sense} with the SST in the NINO3.4 region in the ECHAM5-slab$_{ELNINO}$ simulation as in Fig. 3, but only at lag = 0. SST auto-regression in K/K.

Figure 5.: (a) Power spectrum of the ECHAM5–slab$_{ELNINO}$ simulation and the mean spectrum for the ECHAM5-slab El Nino OFF simulations. (b) Power spectra of different toy models. See text for details.

Figure 6.: NINO3 SST standard deviation (STDV) as function of (a) the mean NINO3 SST and (b) the mean meridional SST difference between NINO3 region minus the mean of the regions 5^0 to north and south for different simulations and observations.

Figure 7.: (a) Spread (root-mean-square error) of the monthly mean SST climatologies in the ECHAM5-slab ensemble relative to the ensemble monthly mean SST climatologies. Units in °C. (b) Same as (a), but for the CMIP3-slab ensemble. (c) The mean difference in the SST of the 6 ECHAM5 simulations with the negative meridional mean SST difference <-1.8°C (as seen in Fig. 6) relative to the ensemble monthly mean SST climatologies. Units in °C. (d) The same as in (c), but for the 2 CMIP3-slab simulations with the negative meridional mean SST difference <-1.5°C. (e) The ratios of the STDV of the 6 simulations as in (c) relative to the

STDV of all ECHAM5 simulations. (f) As in (e), but for the CMIP3-slab ensemble. Each model in the CMIP3-slab analysis contributes to the results with equal weight independent of the length of the simulation.

Figure 8.: (a) The EOF-1 pattern of the ECHAM5-slab El Nino ON simulations. (b) as (a) but for the CMIP3 ensemble. (c) and (d) as (a) and (b) for the El Nino OFF simulations.(e) the DEOF-1 mode of the ECHAM5-slab El Nino ON simulations relative to the El Nino OFF simulations. (f) as (e) but for the CMIP3 ensemble. The explained variances of each EOF-mode in (a) to (d) are shown in the heading. The first percentage values in (e) and (f) are the explained variances of the DEOF-1 modes in the El Nino ON simulations and the second values are for the El Nino OFF simulations.

Figure 9.: (a) Correlation of the total cloud cover with the SST at each grid point for the 18 ECHAM5 simulations with the meridional mean SST difference >-1.8^{o}C (El Nino mode OFF). (b) As in (a) but for 6 ECHAM5 simulations with the meridional mean SST difference <-1.8^{o}C (El Nino mode ON). (c) The difference between (b) minus (a). (d) As in (a) but for all observations. (e) As in (d), but only for the 25% of the coldest monthly mean NINO3 SST. (f) The difference between (e) minus (d). (g) As in (d), but for the CMIP CGCM ensemble. (h) As in (g), but only for the10% of the coldest monthly mean NINO3 SST in the whole CMIP CGCM ensemble. (i) The difference between (h) minus (g). The differences in the central eq. Pacific in (c), (f) and (i) all pass the 99% confidence level of a students t-test.

Figure 10.: Correlation of the total cloud cover with SST over the NINO3 region as function of the (a) mean NINO3 SST and (b) mean meridional SST difference between NINO3 region minus the mean of the regions 5^{0} to north and south for the ECHAM5 simulations. The correlation values are calculated independently for all data pairs with the SST-values within the SST-bin centered on the mean SST value of the points shown in the graph. Anomalies are defined relative to the sample space of each bin. The shaded areas mark the 90% confidence interval. (c) and (d) as in (a) and (b) but for the observations. (e) and (f) as in (a) and (b) but for the whole CMIP model ensemble.

Figure 11.: Correlation of C_{SST} (x-axis) and C_{dSSTdt} (y-axis) with (a) C_{Z20},(b) C_{atmos},(c) C_{solar}, (d) $C_{thermal}$, (e)$C_{latent}$and (f) C_{sense} for the CMIP3 (grey numbers) and CMIP5 (blue numbers) simulations, the observations, the RECHOZ and the ECHAM5-slab$_{ELNINO}$ simulation. The CMIP3 and CMIP5 model names corresponding to the numbers are listed in Tables 1 and 2. The correlations are estimated from the normalized lag -1 to 1 with lag-weighted contributions. See method section for details. Note, that some models are missing in some panels, due to missing data.

Figure 12: Distance (root-mean-square error) of the correlation values as shown in Fig. 11b-f for the CMIP3 (grey numbers) and CMIP5 (blue numbers) simulations, the observations, the RECHOZ and the ECHAM5-

slab$_{ELNINO}$ simulation relative to the observation (x-axis) and the ECHAM5-slab$_{ELNINO}$ simulation (y-axis). Models with incomplete heat flux data are not included in this figure.

Figure 13: Statistics of the CMIP3 BCCR-BCM 2.0 model simulation: (a) and (b) lag/lead cross-correlations with SST as in Fig. 1 and 2, but for the BCCR-BCM 2.0 model simulation. (c) The mean difference in the SST relative to the CMIP3 ensemble mean SST. (d) to (i) Hoevmoeller diagrams along the equatorial Pacific of lag/lead regressions with the SST as in Fig. 3, but relative to the NINO3 region.

Tables

Table 1: List of CMIP3 CGCM models analyzed in this study. The runs without a number in the first column do not have the data for the heat flux analysis as shown in Figure 11. The second column lists the CMIP3-slab simulations as discussed in section 3 with the numbers indicating the lengths of the simulations in years.. The third column lists which of the ECHAM5-slab runs have the Slab Ocean El Nino mode *ON or OFF*, which is also mentioned in column 2 for the CMIP3 slab simulations.

Name	CMIP3-slab	ECHAM5-slab
1. BCCR–BCM2.0	-	**ON**
2. CGCM3.1(T63)	OFF (30yrs)	OFF
3. CGCM3.1(T47)	OFF (30yrs)	OFF
4. CNRM–CM3	-	ECHAM5-slab$_{ELNINO}$
5. CSIRO–Mk3.0	OFF (60yrs)	OFF
6. CSIRO–Mk3.5	-	OFF
7. GFDL–CM2.0	OFF (50yrs)	OFF
8. GFDL–CM2.1	OFF (100yrs)	OFF
9. GISS–AOM	-	OFF
10. GISS–EH	-	**ON**
11. GISS–ER	OFF (120yrs)	OFF
12. IAP–FGOALS–g1.0	-	OFF
13. INM–CM3.0	OFF (60yrs)	**ON**
14. IPSL–CM4	-	OFF
15. MIROC3.2(hires)	OFF (20yrs)	OFF
16. MIROC3.2(medres)	OFF (60yrs)	OFF
17. MIUB–ECHO–G	-	OFF
18. MPI–ECHAM5	OFF (100yrs)	**ON**
19. MRI–CGCM2.3.2	**ON** (150yrs)	OFF
20. UKMO–HadCM3	-	OFF
21. UKMO–HadGEM1	OFF (70yrs)	OFF
ncar_pcm1	-	**ON**
ncar_ccsm3_0	**ON** (50yrs)	OFF
ingv_echam4	-	OFF

Table 2:List of CMIP5 CGCM models analyzed in this study.

Name
1. ACCESS1−0
2. ACCESS1−3
3. BCC−CSM1−1
4. BNU−ESM
5. CanESM2
6. CCSM4
7. CMCC−CM
8. CNRM−CM5
9. CSIRO−Mk3−6−0
10. FGOALS−g2
11. FGOALS−s2
12. GFDL−CM3
13. GFDL−ESM2G
14. GFDL−ESM2M
15. GISS−E2−H
16. GISS−E2−R
17. HadCM3
18. HadGEM2−AO
19. HadGEM2−CC
20. HadGEM2−ES
21. INMCM4
22. IPSL−CM5A−LR
23. IPSL−CM5A−MR
24. MIROC5
25. MIROC−ESM−CHEM
26. MIROC−ESM
27. MPI−ESM−LR
28. MRI−CGCM3
29. NorESM1−ME

Figure 1

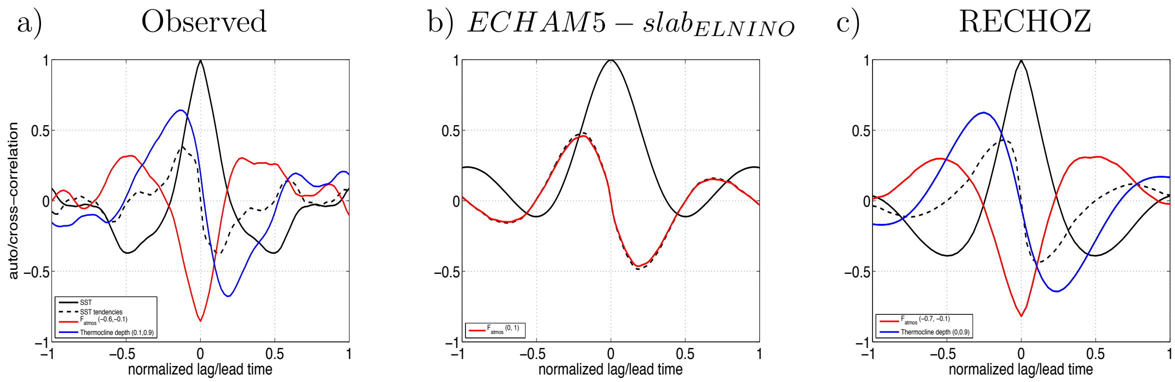

Figure 1.: Lag/lead auto- and cross-correlations with the NINO3 SST. Auto-correlation of the NINO3 SST (solid black line), cross-correlation with the NINO3 SST tendencies (dashed black line), with NINO3 F_{atmos} (red line) and tropical Pacific h (blue line). (a) for observations, (b) for the $ECHAM5 - slab_{ELNINO}$ simulation and (c) for the RECHOZ simulation. The x-axis is normalized by the El Nino oscillation period of each dataset; see methods section for details. The numbers in the legends refer to the correlation values of the forcing curves with the SST and the SST tendency curves, as defined in the methods section.

Figure 2

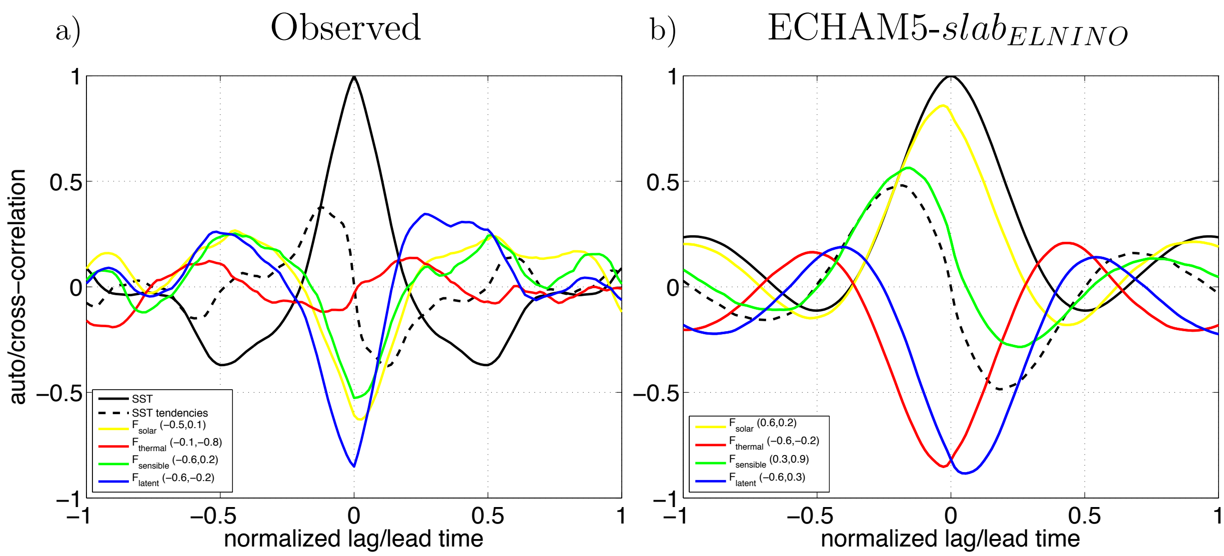

Figure 2.: Lag/lead auto- and cross-correlations with the NINO3 SST, as in Fig. 1, but for cross-correlations with the heat flux components: F_{solar} (yellow), $F_{thermal}$ (red), F_{sense} (green) and F_{latent} (blue). All heat fluxes are defined positive downward. (a) for observations and (b) $ECHAM5 - slab_{ELNINO}$. The two values in brackets are the correlations with SST autocorrelation and SST tendencies curves, respectively.

Figure 3

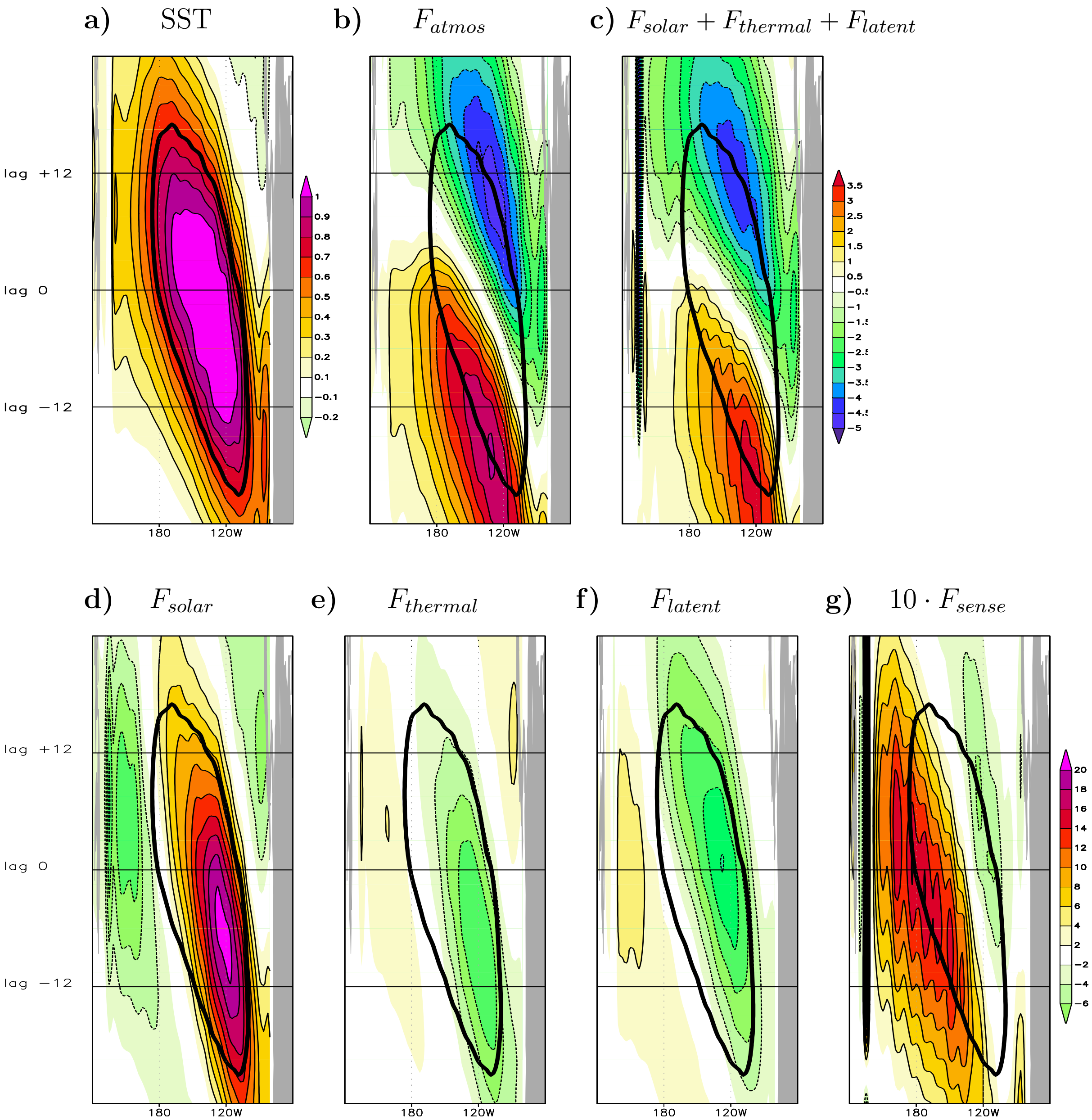

Figure 3.: Hoevmoeller diagrams along the equatorial (3^oS to 3^oN) Pacific of lag/lead regressions with the SST in the NINO3.4 region (170^oW to 120^oW / 5^oS to 5^oN) in the $ECHAM5 - slab_{ELNINO}$ simulation. (a) Auto-regression in [K/K], (b) F_{atmos}, (c) the sum $F_{solar} + F_{thermal} + F_{latent}$, (d) F_{solar}, (e) $F_{thermal}$, (f) F_{latent} and (g) F_{sense}. Values in (b)-(g) are in [W/m2/K]. The y-axis is lag/lead month. The solid thick line in all panels is the 0.7 contour line from (a).

Figure 4

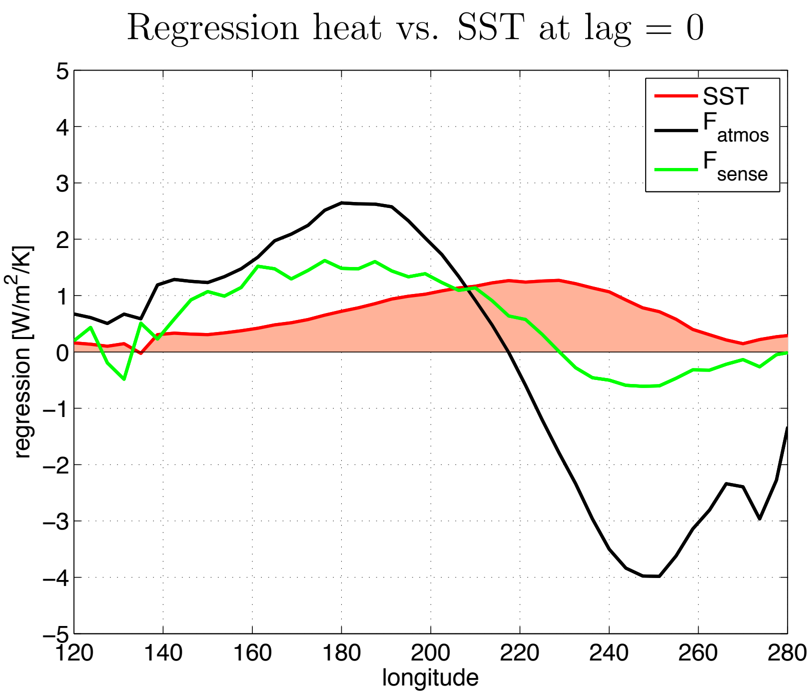

Figure 4.: Regressions of F_{atmos} and F_{sense} with the SST in the NINO3.4 region in the $ECHAM5 - slab_{ELNINO}$ simulation as in Fig. 3, but only at lag = 0. SST auto-regression in K/K.

Figure 5

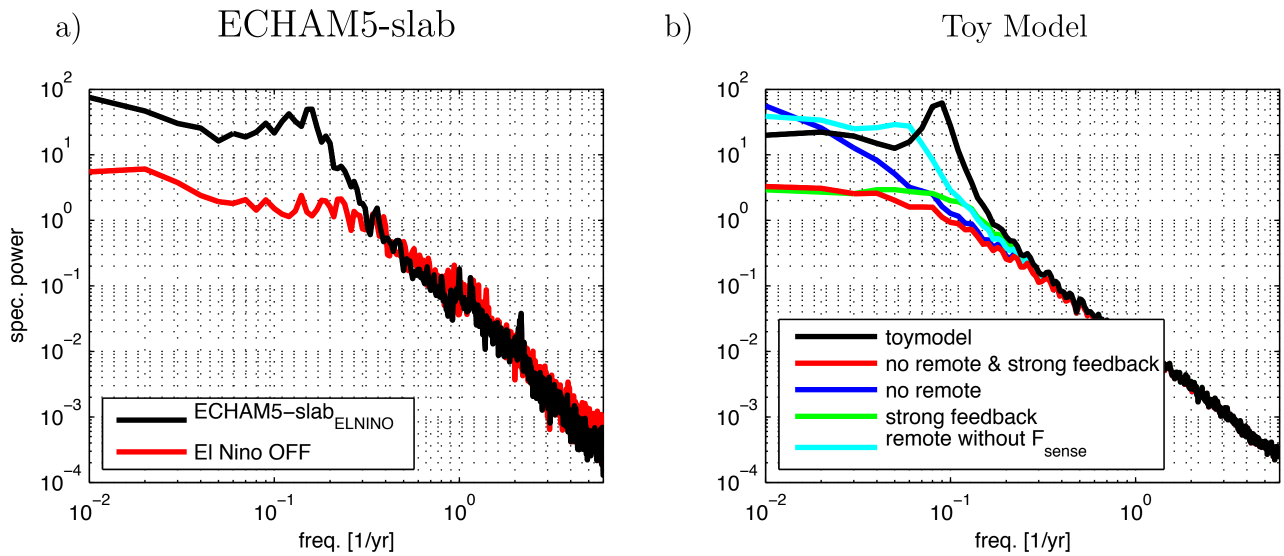

Figure 5: (a) Power spectrum of the $ECHAM5 - slab_{ELNINO}$ simulation and the mean spectrum for the ECHAM5-slab El Nino OFF simulations. (b) Power spectra of different toy models. See text for details.

Figure 6

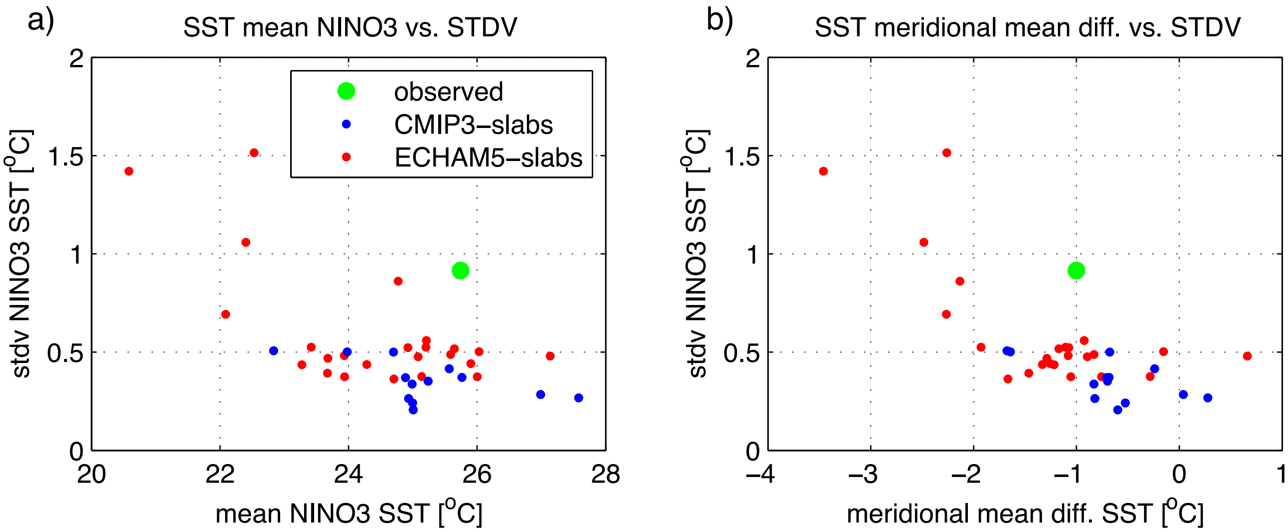

Figure 6: NINO3 SST standard deviation (STDV) as function of (a) the mean NINO3 SST and (b) the mean meridional SST difference between NINO3 region minus the mean of the regions 5^o to north and south for different simulations and observations.

Figure 7

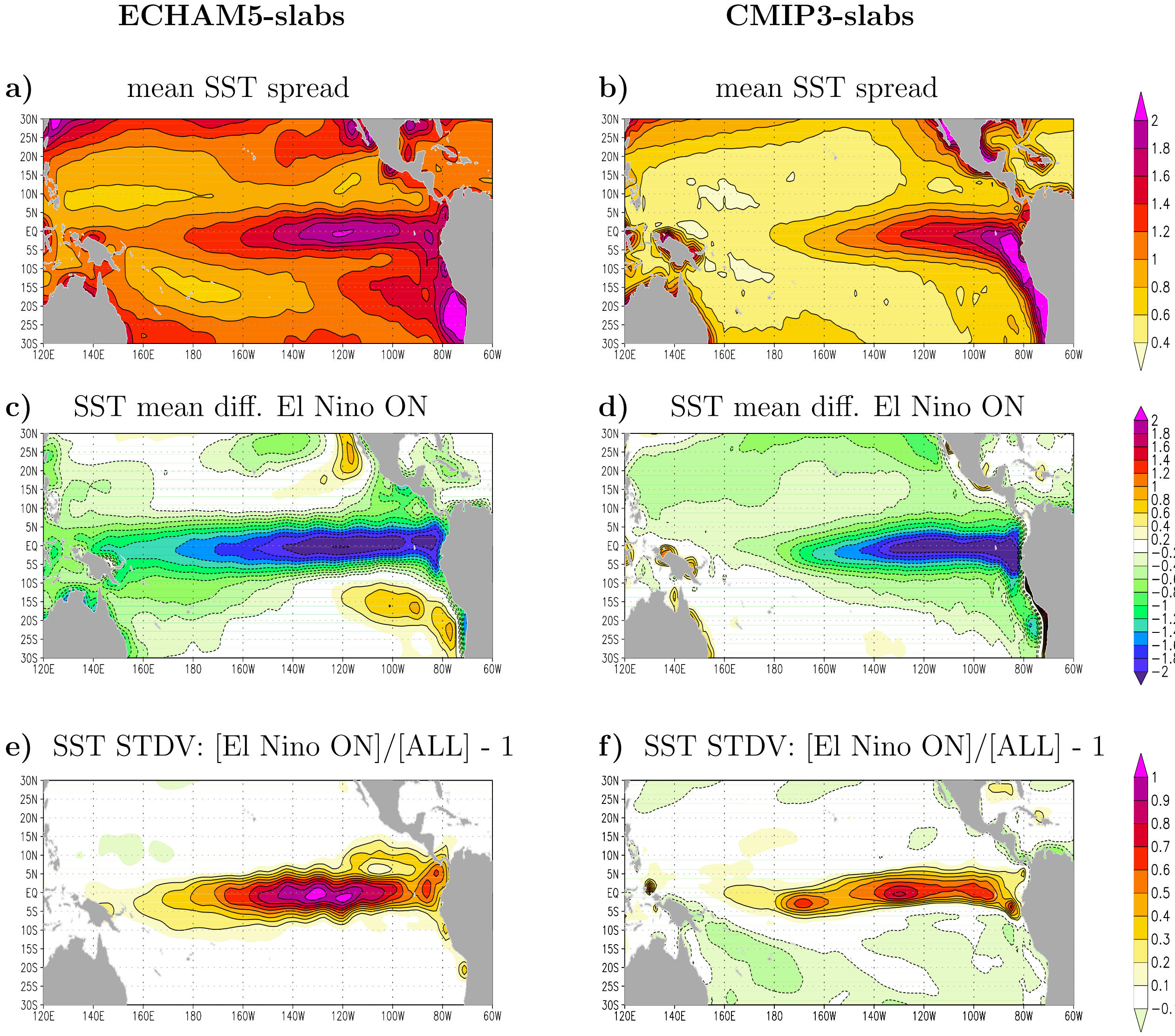

Figure 7: Spread (root-mean-square error) of the monthly mean SST climatologies in the ECHAM5-slab ensemble relative to the ensemble monthly mean SST climatologies. Units in ^{o}C. (b) Same as (a), but for the CMIP3-slab ensemble. (c) The mean difference in the SST of the 6 ECHAM5 simulations with the negative meridional mean SST difference $< -1.8^{o}C$ (as seen in Fig. 6) relative to the ensemble monthly mean SST climatologies. Units in ^{o}C. (d) The same as in (c), but for the 2 CMIP3-slab simulations with the negative meridional mean SST difference ¡-1.5oC. (e) The ratios of the STDV of the 6 simulations as in (c) relative to the STDV of all ECHAM5 simulations. (f) As in (e), but for the CMIP3-slab ensemble. Each model in the CMIP3-slab analysis contributes to the results with equal weight independent of the length of the simulation.

Figure 8

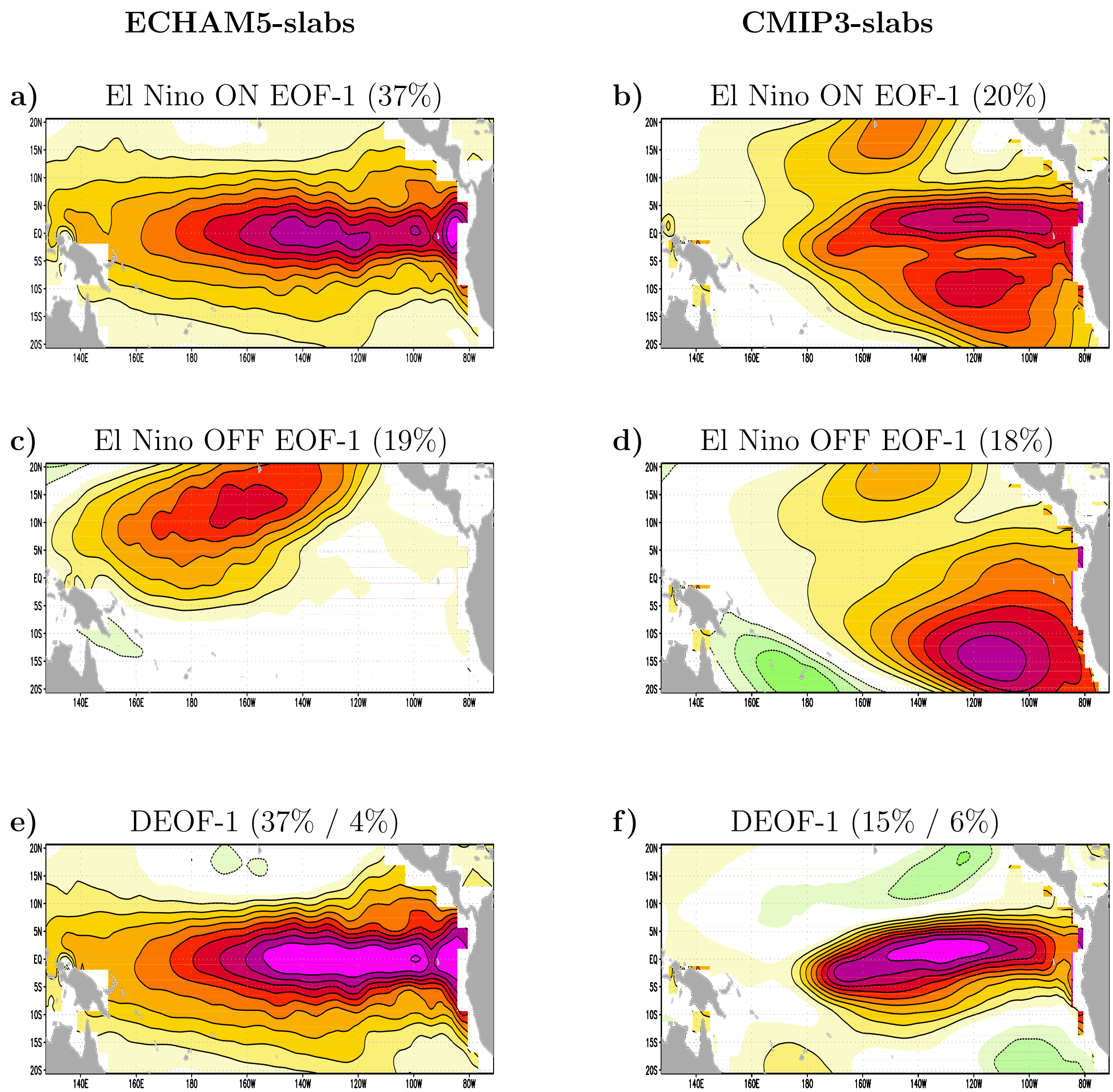

Figure 8.:(a) The EOF-1 pattern of the ECHAM5-slab El Nino ON simulations. (b) as (a) but for the CMIP3 ensemble. (c) and (d) as (a) and (b) for the El Nino OFF simulations. (e) the DEOF-1 mode of the ECHAM5-slab El Nino ON simulations relative to the El Nino OFF simulations. (f) as (e) but for the CMIP3 ensemble. The explained variances of each EOF-mode in (a) to (d) are shown in the heading. The first percentage values in (e) and (f) are the explained variances of the DEOF-1 modes in the El Nino ON simulations and the second values are for the El Nino OFF simulations.

Figure 9

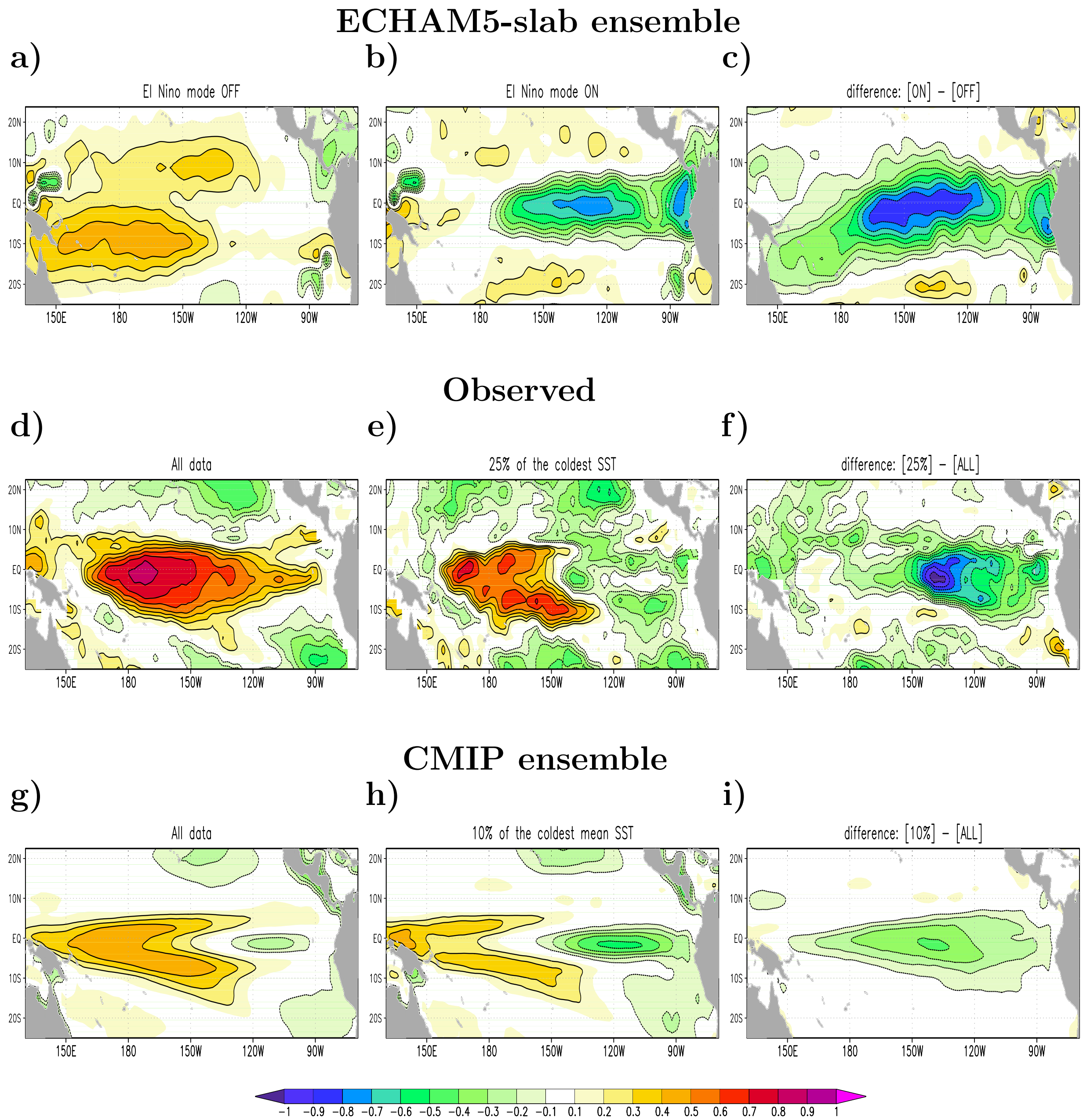

Figure 9: (a) Correlation of the total cloud cover with the SST at each grid point for the 18 ECHAM5 simulations with the meridional mean SST difference $> -1.8^oC$ (El Nino mode OFF). (b) As in (a) but for 6 ECHAM5 simulations with the meridional mean SST difference $< -1.8^oC$ (El Nino mode ON). (c) The difference between (b) minus (a). (d) As in (a) but for all observations. (e) As in (d), but only for those month that are the 25% of the coldest monthly mean NINO3 SST. (f) The difference between (e) minus (d). (g) As in (d), but for the CMIP CGCM ensemble. (h) As in (g), but only for the10% of the coldest monthly mean NINO3 SST in the whole CMIP CGCM ensemble. (i) The difference between (h) minus (g). The difference in in the central eq. Pacific in (c), (f) and (f) all pass the 99% confidence level of a students t-test.

Figure 10

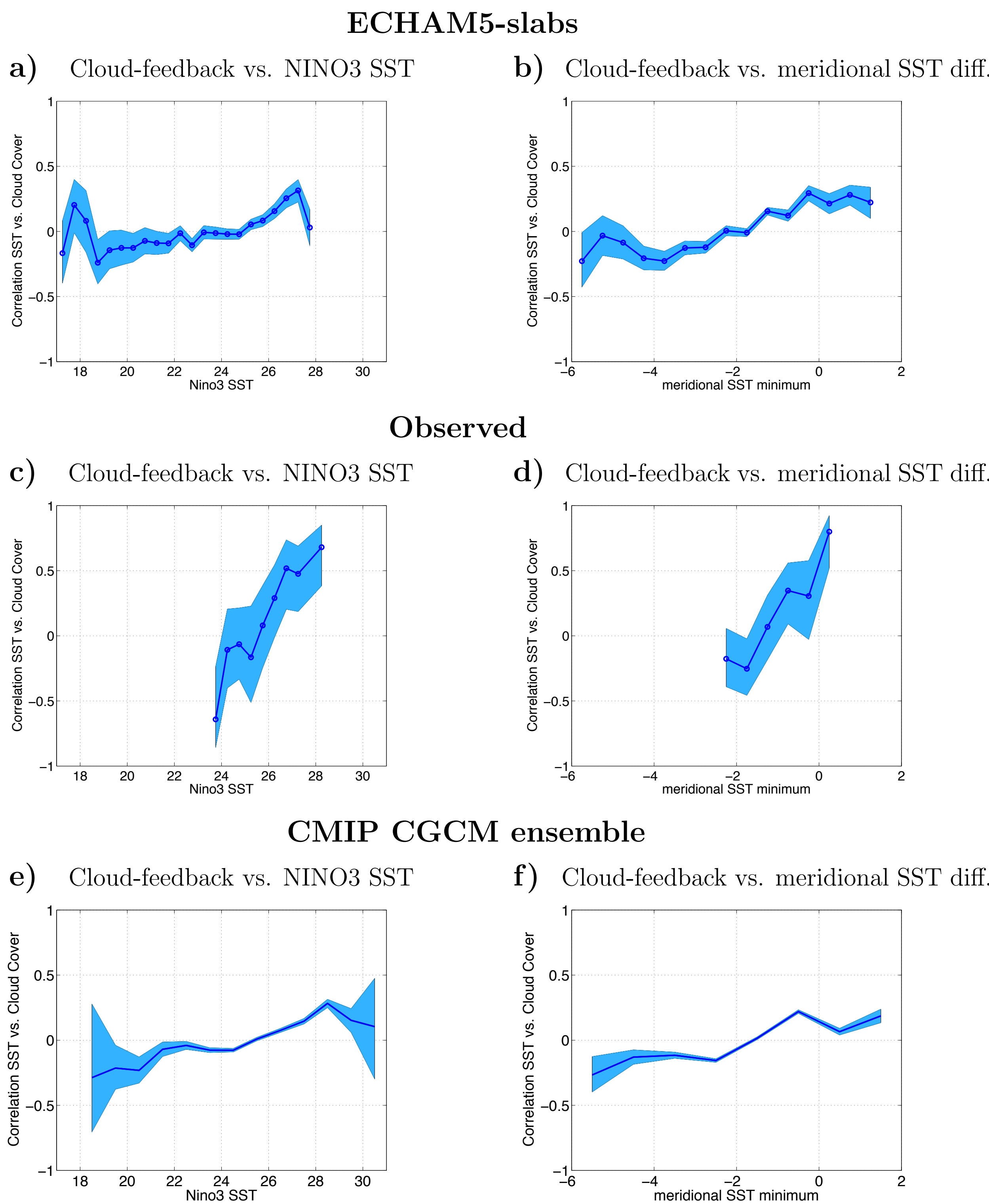

Figure 10: Correlation of the total cloud cover with SST over the NINO3 region as function of the (a) mean NINO3 SST and (b) mean meridional SST difference between NINO3 region minus the mean of the regions 5^0 to north and south for the ECHAM5 simulations. The correlation values are calculated independently for all data pairs with the SST-values within the SST-bin centered on the mean SST value of the points shown in the graph. Anomalies are defined relative to the sample space of each bin. The shaded areas mark the 90% confidence interval. (c) and (d) as in (a) and (b) but for the observations. (e) and (f) as in (a) and (b) but for the whole CMIP model ensemble.

Figure 11

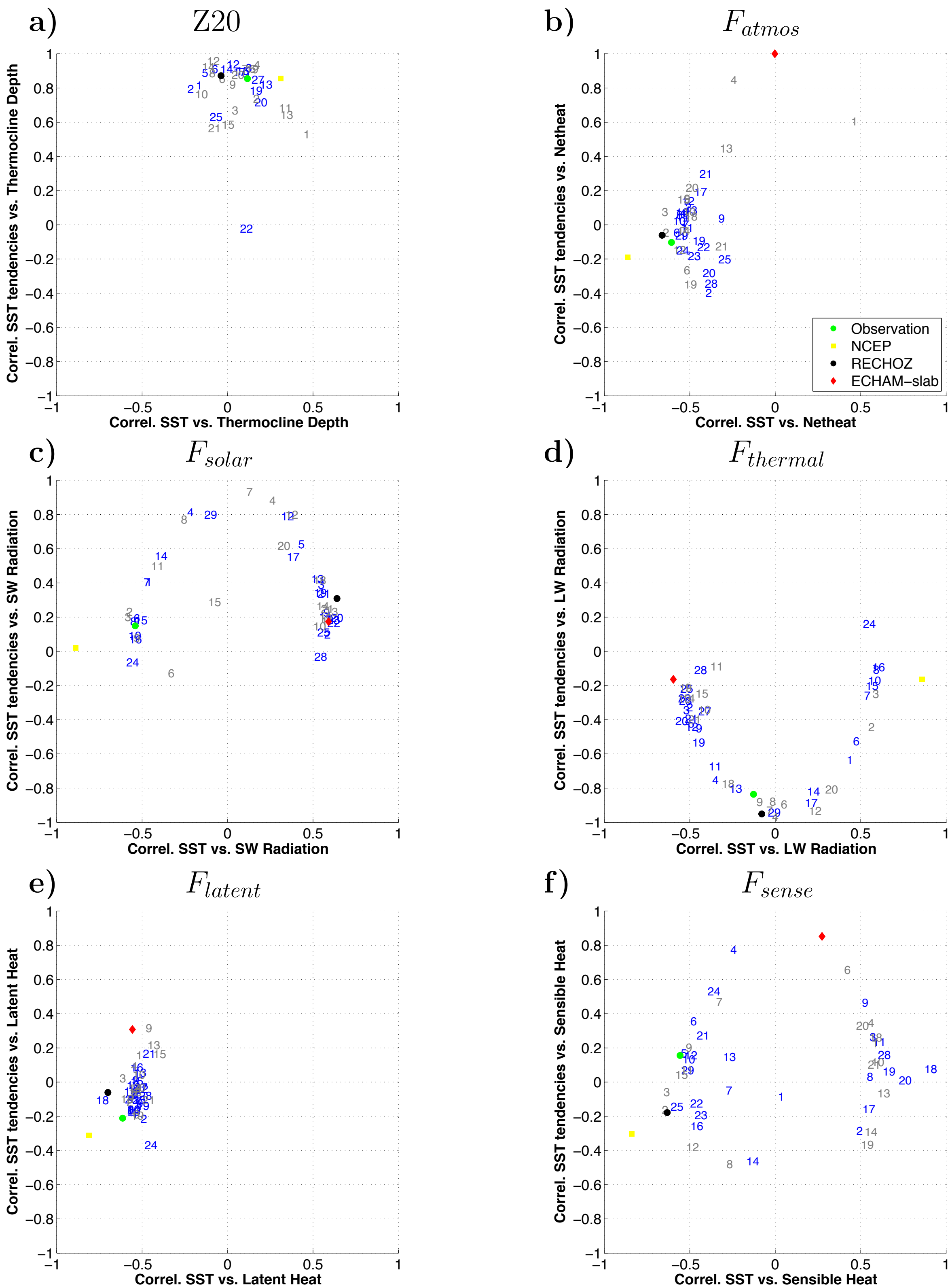

Figure 11: Correlation of CSST (x-axis) and CdSSTdt (y-axis) with (a) C_{Z20}, (b) C_{atmos}, (c) C_{solar} (d) $C_{thermal}$ (e) C_{latent} and (f) C_{sense} for the CMIP3 (grey numbers) and CMIP5 (blue numbers) simulations, the observations, the RECHOZ and the $ECHAM5 - slab_{ELNINO}$ simulation. The CMIP3 and CMIP5 model names corresponding to the numbers are listed in Tables 1 and 2. The correlations are estimated from the normalized lag -1 to 1 with lag-weighted contributions. See method section for details. Note, that some models are missing in some panels, due to missing data.

Figure 12

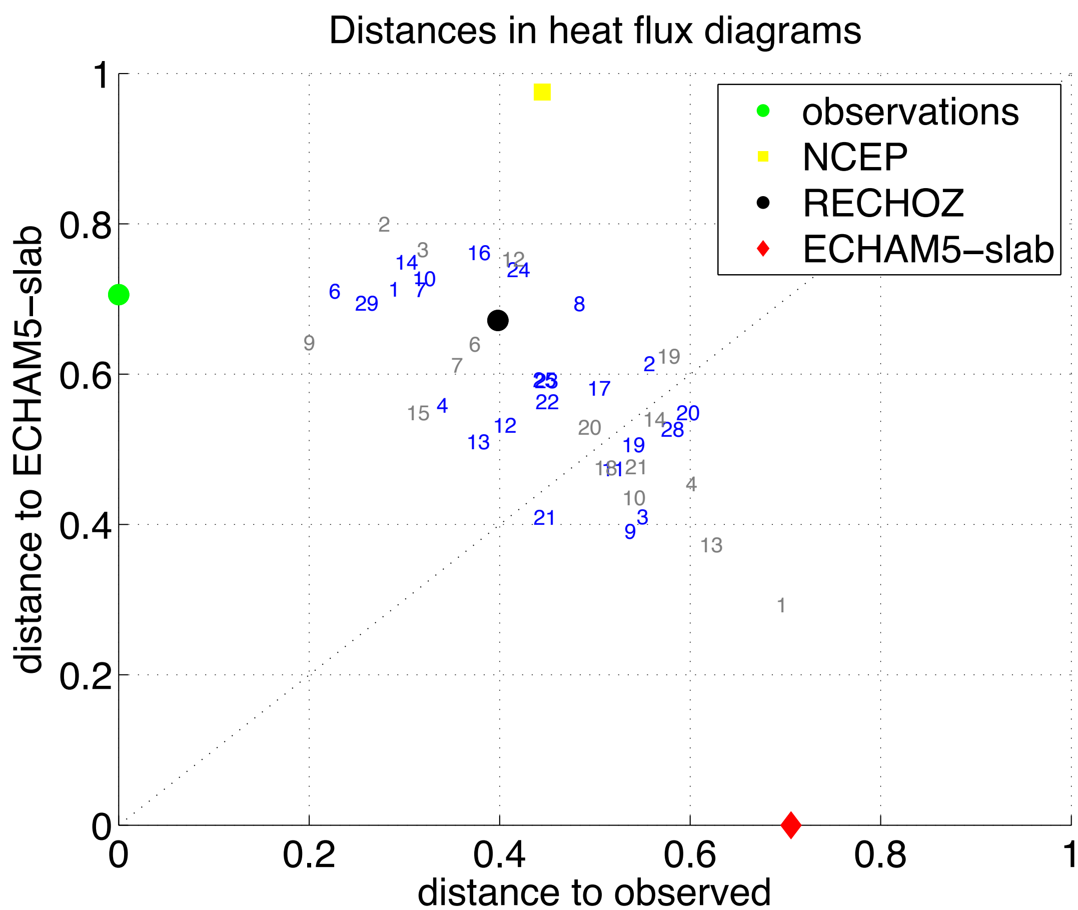

Figure 12: Distance (root-mean-square error) of the correlation values as shown in Fig. 11b-f for the CMIP3 (grey numbers) and CMIP5 (blue numbers) simulations, the observations, the RECHOZ and the $ECHAM5 - slab_{ELNINO}$ simulation relative to the observation (x-axis) and the $ECHAM5 - slab_{ELNINO}$ simulation (y-axis). Models with incomplete heat flux data are not included in this figure.

Figure 13

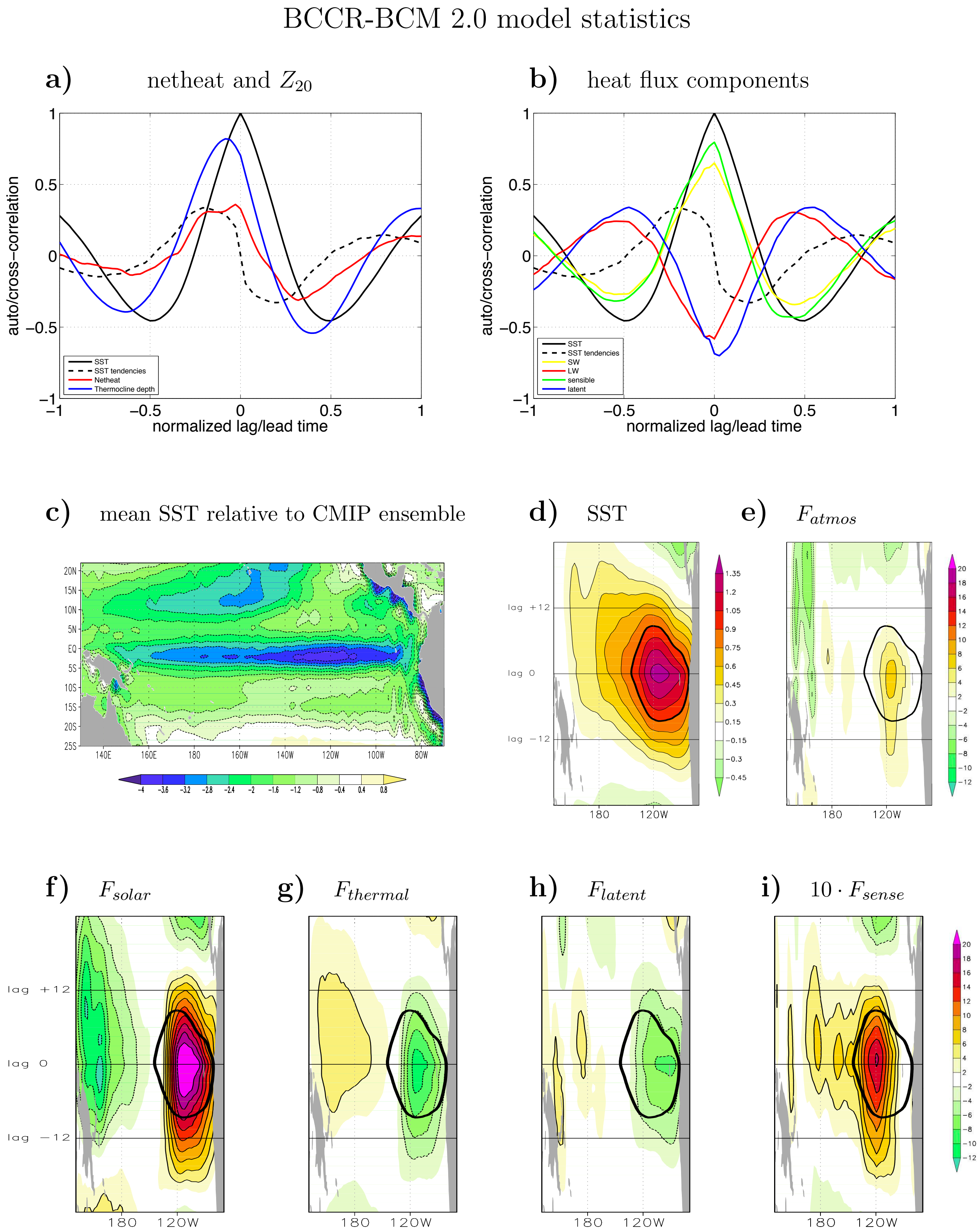

Figure 13: Statistics of the CMIP3 BCCR-BCM 2.0 model simulation: (a) and (b) lag/lead cross-correlations with SST as in Fig. 1 and 2, but relative to the NINO3 region. (c) The mean difference in the SST relative to the CMIP3 ensemble mean SST. (d) to (i) Hoevmoeller diagrams along the equatorial Pacific of lag/lead regressions with the SST as in Fig. 3, but relative to the NINO3 region.